Linköping University Medical Dissertations
No. 970

Calibration of ionization chambers for measuring air kerma integrated over beam area in diagnostic radiology

Factors influencing the uncertainty in calibration coefficients

by

Peter Larsson

Linköping University
FACULTY OF HEALTH SCIENCES

Department of Radiation Physics, IMV, Faculty of Health Sciences,
SE-581 85 Linköping, Sweden

Linköping 2006

The cover was designed by Amelie Karlsson.

Printed in Sweden by LiU-Tryck, Linköping 2006

ISBN: 91-85643-32-7
ISSN: 0345-0082

Till

Erika, Susanna, Tove och Linnea

And since you know you cannot see yourself,
so well as by reflection, I, your glass,
will modestly discover to yourself,
that of yourself which you yet know not of

Shakespeare

ABSTRACT

The air kerma area product P_{KA} is an important quantity used by hospital physicists in quality assurance and optimization processes in diagnostic radiology and is recommended by national authorities for setting of diagnostic reference levels. P_{KA} can be measured using a transmission ionization chamber (kerma area product (KAP) meter) mounted on the collimator housing. Its signal Q_{KAP} must be calibrated to give values of P_{KA}. The objective of this thesis is to analyze the factors influencing the accuracy of the calibration coefficients $k = P_{KA}/Q_{KAP}$ and of reported P_{KA}-values.

Due to attenuation and scatter in the KAP-meter and presence of extra-focal radiation, values of P_{KA} depend on the choice of integration area A and the distance of the reference plane from the focal spot yielding values of P_{KA} that may differ by as much as 23% depending on this choice. The two extremes correspond to (1) $P_{KA}=P_{KA,o}$ integrated over the exit surface of the KAP-meter resulting in geometry independent calibration coefficients and (2) $P_{KA}=P_{KA,Anom}$ integrated over the nominal beam area in the patient entrance plane resulting in geometry dependent calibration coefficients.

Three calibration methods are analysed. Method 1 aims at determine $P_{KA,Anom}$, for clinical use at the patient entrance plane. At standard laboratories, the method is used to calibrate with respect to radiation incident on the KAP-meter. Problems with extra-focal and scattered radiation are then avoided resulting in calibration coefficients with low standard uncertainty (±1.5 %, coverage factor 2). Method 2 was designed in this work to approach determination of $P_{KA,o}$ using thermoluminescent detectors to monitor contributions from extra-focal radiation and account for the heel effect. The uncertainty in derived calibration coefficients was ± 3% (coverage factor 2). Method 3 uses a Master KAP-meter calibrated at a standard laboratory for incident radiation to calibrate clinical KAP-meters. It has potential to become the standard method in the future replacing the tedious method 2 for calibrations aiming at determination of $P_{KA,o}$.

Commercially available KAP-meters use conducting layers of indium oxide causing a strong energy dependence of their calibration coefficients. This dependence is investigated using Monte Carlo simulations and measurements. It may introduce substantial uncertainties in reported P_{KA}– values since calibration coefficients as obtained from standard laboratories are often available only at one filtration (2.5 mm Al) as function of tube voltage or HVL. This is not sufficient since higher filtrations are commonly used in practice, including filters of Cu. In extreme cases, calibration coefficients for the same value of HVL but using different tube voltages and filtrations can deviate by as much as 30%. If standardised calibration methods are not used and choice of calibration coefficients not carefully chosen with respect to beam quality, the total uncertainty in reported P_{KA}–values may be as large as 40-45%. Conversion of P_{KA}-values to risk related quantities is briefly discussed. The large energy dependence of the conversion coefficients, ε/P_{KA}, for determination of energy imparted, ε, to the patient reduces to a lower energy dependence of calibration coefficients $C_{Q,\varepsilon} = \varepsilon/Q_{KAP}$ for determination of ε from the KAP-meter signal.

CONTENTS

1. INTRODUCTION 9

2. COST AND BENEFIT IN X-RAY DIAGNOSTICS- CONCEPTS USED FOR RISK ESTIMATES 10

2.1. RISK-RELATED QUANTITIES 10
2.1.1. Effective dose, E 10
2.1.2. Energy imparted to the patient, ε 10
2.2. MEASURABLE QUANTITIES 11
2.2.1. Entrance surface dose (ESD) 11
2.2.2. Kerma area product (P_{KA}) 11
2.3. DIAGNOSTIC REFERENCE LEVELS, DRL 12

3. THE AIMS OF THIS STUDY 13

4. THEORETICAL CONSIDERATIONS 15

4.1. DEFINITION OF THE AIR-KERMA AREA PRODUCT P_{KA} 15
4.1.1. The spatial distribution of $K_{c,air}$ 15
4.1.2. Reference plane and area of integration 17
4.2. THE KAP-METER 18
4.2.1. The ideal KAP-meter 19
4.2.2. The real KAP-meter 19

5. CALIBRATION PROCEDURES 21

5.1. METHOD 1, USING A NOMINAL BEAM AREA 21
5.1.1. Determination of A_{film} 23
5.1.2. Dependence of A_{film} on optical density 24
5.1.3. Interobserver variations in estimates of A_{film} 24
5.2. METHOD 2, ESTIMATE FROM INTEGRATION 26
5.2.1. Equipment 26
5.2.2. The calibration procedure 27
5.2.3. The calibration coefficient k_2 29
5.3. METHOD 3, USING A MASTER KAP-METER 31
5.4. COMPARISONS OF CALIBRATION METHODS 1 AND 2 32
5.4.1. Calibrations according to method 1 in an experimental laboratory 32
5.4.2. Calibrations according to method 1 at clinical x-ray installations 34
5.5. COMPARISONS OF METHODS 1 AND 3 37
5.6. CALIBRATION AT UNDERCOUCH INSTALLATIONS 37
5.6.1. Correction of over-couch calibration coefficients 37
5.6.2. A new calibration coefficient derived using a Master KAP-meter 38

6. ENERGY DEPENDENCE OF THE KAP-METER CALIBRATION COEFFICIENT 41

6.1. THE SENSITIVITY (*S*) AND THE FIELD HOMOGENEITY FACTOR (*F*) 43
6.2. MONTE CARLO SIMULATIONS 44
6.2.1. Monte Carlo codes 44
6.2.2. Simulations using MCNP 44
6.2.3. Simulations with the Pencyl code from PENELOPE 46
6.3. MEASUREMENTS OF SENSITIVITY, *S* 46
6.3.1. Equipment used in the measurements 46
6.3.2. Added filter on top of the KAP-meter 48

6.4. RESULTS AND DISCUSSION 48
6.4.1. Effects of KAP-meter wall material, and atomic composition and thickness of conducting layers *48*
6.4.2. Influence from choice of reference plane and area of integration *53*
6.4.3. Comparison between experimental results and Monte Carlo simulations *56*
6.4.4. Variation of the calibration coefficients *58*
6.5. EFFECTS OF ADDED FILTERS ON KAP-METER CALIBRATION COEFFICIENTS 61

7. ESTIMATION OF UNCERTAINTIES 63

7.1. UNCERTAINTY IN THE CALIBRATION COEFFICIENT, K_2 63
7.2. UNCERTAINTIES IN COMPARISONS OF CALIBRATION COEFFICIENTS 65
7.3. UNCERTAINTIES IN THE WORKSHOP CALIBRATION COEFFICIENT 66
7.4. EXPANDED UNCERTAINTY 67
7.5. UNCERTAINTIES IN REPORTED P_{KA}-VALUES 67

8. RADIATION RISK AND P_{KA} 69

8.1. $P_{KA,PATIENT}$ 69
8.2. CONVERSION TO RISK RELATED QUANTITIES 70

9. SUMMARY 72

10. CONCLUSIONS 73

11. FUTURE WORK 74

ACKNOWLEDGEMENTS 75

REFERENCES 76

PREFACE

This thesis is based on the following papers:

I Larsson J P, Persliden J, Sandborg M and Alm Carlsson G 1996 Transmission ionization chambers for measurements of air collision kerma integrated over beam area. Factors limiting the accuracy of calibration. *Phys. Med. Biol.* **41** 2381-2398 *

II Larsson J P and Alm Carlsson G 1996 Evaluation of the uncertainties in KAP-meter calibrations. Report 82, ISRN LiU-RAD-R--82—Se

III Larsson J P, Persliden J and Alm Carlsson G 1998 Ionization chambers for measuring air kerma integrated over beam area. Deviations in calibration values using simplified calibration methods. *Phys. Med. Biol.* **43** 599-607 *

IV Malusek A, Larsson J P and Alm Carlsson G 2006 Monte Carlo study of the dependence of the KAP-meter calibration coefficient on beam aperture, x-ray tube voltage, and reference plane. Submitted for publication in *Phys. Med. Biol.*

V Larsson J P, Malusek A, Persliden J and Alm Carlsson G Energy dependence in KAP-meter calibration coefficients: Dependence on calibration method, type of KAP-meter, and added filter close to the KAP-meter. To be submitted for publication in *Phys. Med. Biol.*

* Reprints have been included with permission from the publisher

Preliminary reports of this thesis were given at:

International Atomic Energy Agency (IAEA) International Symposium on Measurement Assurance in Dosimetry, Vienna. (24-27 may 1993)

Läkaresällskapets riksstämma. Stockholm, Sweden. (30 November 1995)

1. Introduction

X-rays discovered in 1895 by Wilhelm Konrad Röntgen were very soon afterwards used for various purposes in medicine. The differing absorption properties of x-rays in different tissues made it possible, for the first time, to image inside the human body. At this time, no one was aware of the harmful effects of x-rays and they were used extensively. As a consequence, many of the pioneers who used x-rays suffered severe radiation injuries.

Today, the hazards of ionizing radiation are well-known and their effects are divided into two categories, deterministic and stochastic (ICRP 1991).

Deterministic effects occur when the number of cells killed due to irradiation cannot be compensated for by cell proliferation resulting in loss of function in tissues or organs. The severity of deterministic effects increases with increasing absorbed dose. Depending on the type of effect threshold values in the range 1-10 Gy exist. Below these deterministic effects do not appear.

Stochastic effects are those caused by non-lethal alterations in normal cells which can give rise to malignant conditions. The probability of malignancy is related to the absorbed dose, while the severity of the cancer is not. The latency time is several years. Threshold values are assumed not to exist and risks to increase with increasing absorbed dose. The effect on the population can be deduced from the collective effective dose. For instance, at the University Hospital in Linköping, the collective dose from roentgen examinations of about 100 manSv per year gives rise to an estimated number of 5 fatal cancers per year (calculated using the probability coefficient 0.05 Sv^{-1} for fatal cancer recommended in ICRP (1991)).

2. Cost and benefit in x-ray diagnostics- concepts used for risk estimates

Illness implies a risk for the patient. If an x-ray examination is made and a proper treatment can be received, this risk may be radically reduced (Edholm 1982). Even if a net benefit is usually achieved, the examination should be optimized so that sufficient information is obtained at the lowest possible absorbed dose (the ALARA-principle, As Low As Reasonable Achievable) (ICRP 1991).

Although recently cases in wich patients suffered from deterministic skin injuries in x-ray imaging have been reported (FDA 1994, Koenig *et al* 2001) the risk of stochastic effects is the main concern, i.e. the enhanced risk of developing cancer or hereditary injury as a consequence of irradiation.

An important first step in minimising risk is to find methods of monitoring the risk by means of suitable risk-related quantities.

2.1. Risk-related quantities

Two quantities, the effective dose, E, and the energy imparted, ε, to the patient have frequently been used to estimate stochastic risks in diagnostic roentgen examinations.

2.1.1. Effective dose, E

The effective dose (ICRP 1991) is a quantity that is defined to correlate with the stochastic risk of an irradiation. It takes into account the effects of radiation quality and tissue sensitivity by radiation- and tissue-weighting factors, w_R and w_T. In practice, E has to be derived from quantities which can easily be measured in the clinic.

2.1.2. Energy imparted to the patient, ε

The mean energy imparted to the total body or to a specified volume can be determined from (Alm Carlsson 1985)

$$\varepsilon = \overline{R}_{in} - \overline{R}_{out} + \overline{\sum Q}$$

R_{in} and R_{out} are the radiant energies incident on and escaping from the volume. $\sum Q$ is the net change in the rest mass energy of nuclei or elementary particles occurring within the volume. In the case of diagnostic x-rays, $\sum Q$ is zero. The bars indicate expectation values.

Energy imparted is not as closely related to the risk as effective dose, but has the advantage of being independent of the current values of the weighting factors. In many practical situations, ε represents a risk estimate which is as realistic as the effective dose E

(Shrimpton and Wall 1982) since the complexity involved in deriving E necessitates a number of assumptions and simplifications. In practice, both E and ε have to be derived from quantities which are easy to measure clinically.

It should be noted that tabulated organ doses derived from Monte Carlo simulations have up to now been derived using a broad range of beam qualities (tube voltages and filtrations) but often only one fixed beam-area for each projection. However, in the Monte Carlo program PCXMC (Tapiovaara *et al* 1997) it is possible to calculate the effective dose for arbitrary beam areas and beam positions.

2.2. Measurable quantities

2.2.1. Entrance surface dose (ESD)

ESD can be measured directly and related to effective dose or energy imparted to the patient by means of tabulated organ doses (Hart *et al* 1994, Hart *et al* 1996) based on Monte Carlo simulations in anthropomorphic phantoms. Contrary to *E*, *ESD* is insensitive to changes in the x-ray beam area and is only meaningful to use in connection with single projection radiographs, i.e., it is of limited use in examinations involving fluoroscopic procedures.

ESD is recommended by NRPB (1992) as one of the quantities to be measured in patient dose estimations. In the "European Guidelines on Quality Criteria for Diagnostic Radiographic Images" (EUR 1996a, EUR 1996b), dose criteria are given in terms of reference levels of *ESD* for a standard-sized patient.

2.2.2. Kerma area product (P_{KA})

The air kerma area product (P_{KA}) can be measured using a plane-parallel transmission ionisation chamber (Pychlau and Pychlau 1964, Carlsson 1965a) mounted in front of the x-ray tube and covering the entire beam. Properly calibrated, the chamber (kerma area product meter, KAP-meter) measures the air-collision kerma integrated over the beam area, P_{KA}, the determination of which is discussed in detail in section 4.1. An alternative to using a KAP-meter is to let the computer controlling the x-ray settings calculate the P_{KA} from knowledge of collimator position, tube current, tube voltage and filtration. This alternative also requires an independent determination of P_{KA} (as described in section 5) in order to establish the relation between P_{KA} and the parameters used in calculating it (collimator positions, tube current, tube voltage and filtration).

The P_{KA} -value can be related to the energy imparted to the patient via published conversion factors (Carlsson 1963, Alm Carlsson *et al* 1984, Månsson *et al* 1993, Persliden and Sandborg 1993). Like *ESD*, it can be related to effective dose using tabulated organ doses (Le Heron 1992, Månsson *et al* 1993, Hart *et al* 1994, Hart and Wall 1994, Hart *et al* 1996). This quantity has several advantages, e.g., it is easily measured routinely, it can be

used for complete examinations (including fluoroscopy procedures) and it registers variations in beam area. The P_{KA} -value is recommended by the FDA (1994) and the NRPB (1992) for monitoring patient doses and, being more closely related to effective dose than the entrance surface dose (Le Heron 1992), it is important in the optimization process.

2.3. Diagnostic reference levels, DRL

A predecessor to DRL was introduced in a report from the National Radiological Protection Board (NRPB) in the United Kingdom (NRPB 1990) as a tool to recognize abnormally high doses in conventional x-ray examination procedures. Later the concept of DRL was adopted by the International Commission on Radiological Protection (ICRP) in their publication ICRP 73 (ICRP 1996) and was also mentioned in a directive from the Council of the European Union on Medical Exposure (EuropeanCouncil 1997) stating that " Member states shall: promote the establishment and the use of diagnostic reference levels for radiodiagnostic examinations,...". According to recommendations, the selected values of DRL should be specific to a country or region and are typically chosen as a percentile of an observed distribution of values for a specific type of examination procedure. In several national guidelines e.g. in Sweden, Denmark, Germany and USA (Leitz and Jönsson 2001, Leitz 2004), the air kerma area product is one of recommended quantities for reporting DRL. A harmonization of the calibration procedures within, at least, the same region or country is therefore desirable since calibration coefficients derived using different calibration methods can deviate as much as 40-45% (Paper V).

3. The aims of this study

To present a theoretical basis for the choice of reference plane and area of integration for determining P_{KA}.

To describe and perform a geometry independent method for KAP-meter calibration (method 2), to consider carefully factors contributing to the uncertainties in the calibration coefficients and to identify and quantify different sources of errors.

To compare calibration coefficients derived using the geometry independent calibration method (method 2) and an easy-to-perform calibration method commonly used in clinical practice (method 1) and to assess the effects of different parameters on the calibration coefficients derived using method 1.

To assess the influence of radiation scattered from filters and from the KAP-meter on the calibration coefficients.

To describe and quantify the dependence of calibration coefficients on the photon energy spectrum and to explain the basic mechanisms of this dependence in different types of KAP-meters.

To briefly address the relationship between P_{KA} and patient risk related quantities.

4. Theoretical considerations

This section is introduced to serve as an introduction in general to KAP-meter measurements and to the specific problems that have to be handled while setting-up of a calibration method. It should also facilitate a proper analysis and discussion of the influences of the energy spectrum and scattered radiation on the calibration coefficient.

4.1. Definition of the air-kerma area product P_{KA}

The air kerma area product, P_{KA}, is defined as (IAEA 2006)

$$P_{\mathrm{KA}} = \int_A K_{\mathrm{c,air}}\, \mathrm{d}A, \qquad (1)$$

where A is the area of the beam in a reference plane (e.g. the patient entrance plane) perpendicular to the beam axis, and $K_{c,air}$ is the air collision kerma at that plane. Provided attenuation and scatter of photons in the primary beam can be neglected, the value of P_{KA} is independent of the distance of the reference plane from the focal spot. This statement is valid also for an extended x-ray source provided the integration over the area A is extended to include the extra-focal radiation (see figure 1c).

In practice, photons in the primary beam are scattered in the air, in the filter, and in the KAP-meter. Scattered photons are spread in all directions (solid angle 4π) and the value of P_{KA} thus depends on the choice of reference plane and area of integration. The determination of P_{KA} also requires knowledge of the spatial distribution of $K_{\mathrm{c,air}}$ in the area selected. These three factors (reference plane, area of integration, distribution of $K_{\mathrm{c,air}}$) are discussed in subsequent sections.

4.1.1. The spatial distribution of $K_{c,air}$

The distribution of $K_{\mathrm{c,air}}$ is affected mainly by four factors:

1. Because of the inverse square law and attenuation in the filter, $K_{\mathrm{c,air}}$ at the edges of the beam area A is lower than on the central axis due to the larger distances from the focal spot to points on the edge of the beam as well as to the increased attenuation of photons passing obliquely through any added filters, Figure 1a.
2. The heel effect: Due to differences in anode filtration for photons emitted in different directions, the photon energy spectrum and $K_{\mathrm{c,air}}$ vary with position in the beam. $K_{\mathrm{c,air}}$ decreases but the mean energy of the photons increases towards the anode side of the beam, Figure 1b.

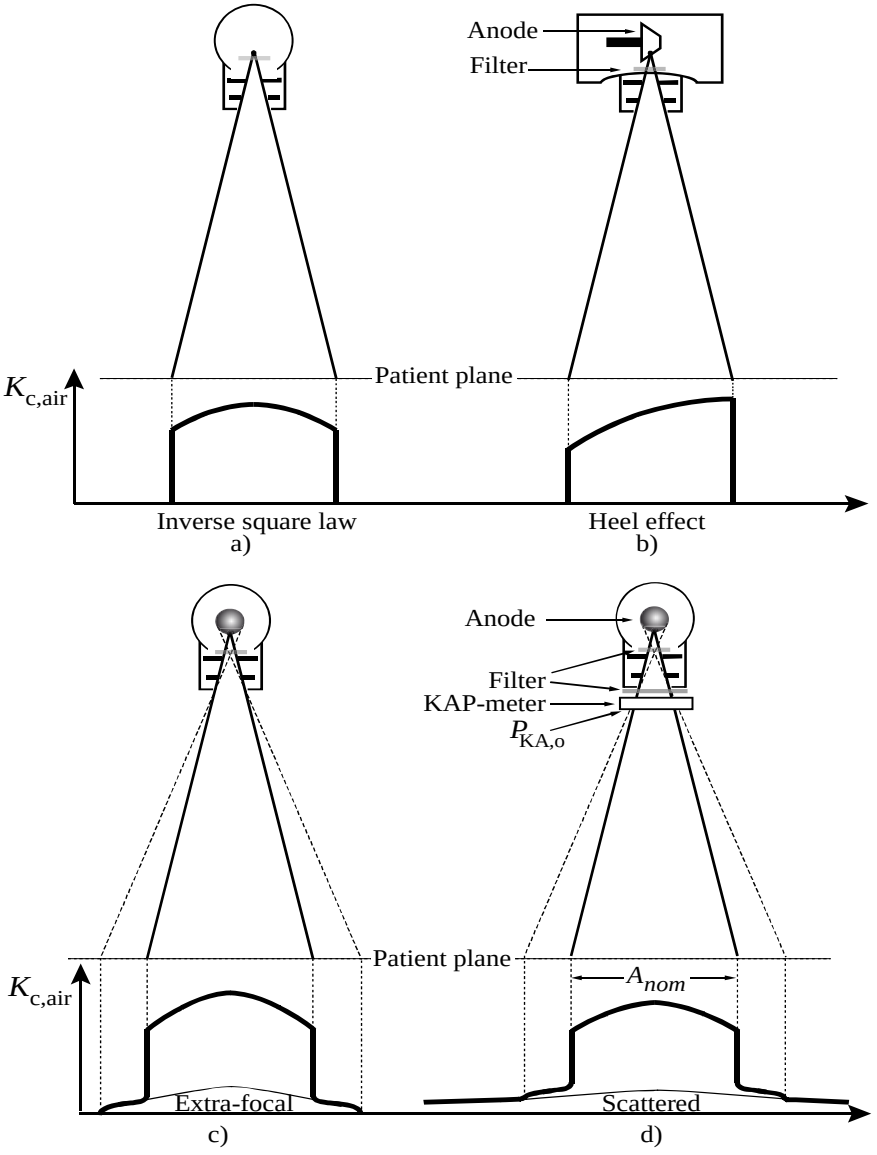

Figure 1. Schematic representations of the $K_{c,air}$ profiles in a plane perpendicular to the central axis in four different cases. a) In the ideal case with a point focal spot with isotropic emission, $K_{c,air}$ decreases towards the edges of the beam due to the longer distances from the focal spot. b) The heel effect causes different attenuation in the anode of the photons emerging at different angles and results in $K_{c,air}$ variations in the anode-cathode direction. Here, unlike in a), c), and d) the profile along the anode-cathode direction is shown. c) The effect of extra-focal radiation. The whole anode acts as an extended source of extra-focal photons. d) The effect of scattering from any filters ”downstream” of the collimating device, KAP-meter and collimators. The scattered photons contribute to the $K_{c,air}$ distribution and are spread over a large area inside and outside the nominal beam area.

3. Extra-focal radiation: Due to electrons impinging on the anode but outside the focal spot, the whole anode plate acts as a photon source. Photons reaching the patient plane which do not emanate directly from the focal spot but from locations "upstream" of the last pair of collimators (i.e. the collimators most distant from the focal spot) are included in the term “extra-focal radiation”. For example, this could include photons from interactions in the glass of the exit window of the x-ray tube, in the mirror and at the collimator edges. The magnitude and distribution of the extra-focal radiation depend strongly on the geometry of the collimators. Extra-focal radiation is spread inside and beyond the nominal beam area A_{nom} defined by the primary beam, figure 1c. With poor collimation, extra-focal radiation can amount to 20% or more (Ardran and Crooks 1978).
4. Scattered radiation from the KAP-meter walls and any filters positioned "downstream" of the collimators: Scattered radiation is spread inside but also over a large area outside the nominal beam, Figure 1d. Its magnitude and distribution depend on filter material and thickness, beam area, distance between the filter and the plane of measurement, tube voltage and primary filtration (i.e. the filter positioned close to the exit window of the x-ray tube “upstream” of the collimators).

4.1.2. Reference plane and area of integration

Three different areas of integration and reference planes are discussed here.

1. A_{nom} at the patient plane: Conventionally the area is defined as the area within 50% of the maximum optical density on a film positioned perpendicular to the central axis of the beam at a position “just above the couch” (NRPB 1992). A_{nom} corresponds approximately to the area defined by the primary beam and the resulting air kerma area product is denoted by $P_{KA,Anom}$. This concept excludes photons outside A_{nom} (extra-focal and scattered radiation) that may significantly contribute to the radiant energy incident on the patient. The fraction of photons outside A_{nom} depends on the geometry, i.e. on the distance from the focal spot, beam area and the construction of the collimating system. In addition, scattered photons from the KAP-meter itself and from any additional filters close to the KAP-meter contribute significantly to the fraction of photons outside A_{nom}.
2. The entire plane: The use of this concept was suggested in Paper I in order to arrive at a value of P_{KA} that is independent of the distance from the focal spot, when the attenuation and scattering of photons in air are neglected. However, the Monte Carlo simulations in Paper IV of the radiation scattered from the KAP-meter and the filter positioned close to it (Figure 1d) show that, as a function of the radius of the integration area, P_{KA} converges only slowly to a saturation value or may even diverge when vacuum is assumed.

3. The exit surface of the sensitive volume of the KAP-meter: This alternative definition of the integration area was suggested in Paper IV. It is well suited for Monte Carlo simulations and includes all photons scattered in the filter and in the KAP-meter that may eventually hit the patient. The resulting air kerma area product is denoted $P_{KA,o}$ (where the index "o" stands for "out"). Another advantage with $P_{KA,o}$ is its close relation to Q_{KAP} since most of the photons passing through the exit surface of the KAP-meter have passed through its sensitive volume. $P_{KA,o}$ corresponds to the quantity measured by an ideal KAP-meter (section 4.2.1.) and is in fair agreement with the value of P_{KA} measured with a chamber calibrated using a Master KAP-meter (where the Master KAP-meter is calibrated at a primary standard laboratory), see section 5.3. Provided attenuation and scatter in air can be neglected, $P_{KA,o}$ will give the same value of P_{KA} in the patient plane although spread over a larger area with some of the photons possibly passing beside the patient. When using values of $P_{KA,o}$ in risk estimates the fraction of photons passing beside the patient, and thus not contributing to the radiant energy incident on the patient, should be accounted for. In the special cases where undercouch configurations are used, further corrections are needed in order to keep P_{KA} related to the radiant energy incident on the patient.

4.2. The KAP-meter

The instrument of choice in measurements of P_{KA} is a plane-parallel transmission ionization chamber mounted on the collimator housing and covering the entire x-ray beam (Pychlau and Pychlau 1964, Carlsson 1965a). KAP-meters differ from common ionization chambers in two aspects. First, their sensitive air volumes are only partly irradiated during measurements and, second, KAP-meters used for clinical measurements should be calibrated to indicate the "outgoing" air kerma area product (downstream of the chamber) in order to be linked to the radiant energy incident on the patient and ultimately, patient risk.

The calibration coefficient, k, is in general defined as

$$k = \frac{P_{KA,r}}{Q_{KAP}}, \qquad (2)$$

where Q_{KAP} is the electric charge collected by the KAP-meter and P_{KA} is the air kerma area product for a given area of integration, A, in a reference plane r perpendicular to the beam axis and traversed by photons transmitted through the KAP-meter. The choice of reference plane and integration area, i.e., the choice of calibration method, influences the value of the calibration coefficient (section 4.1.2.).

4.2.1. The ideal KAP-meter

An ideal KAP-meter has air equivalent walls of a thickness that allows electronic equilibrium to be established in the sensitive air volume. The walls are so thin that they do not attenuate incident photons. In practice, these two conditions can never be fulfilled but, since the mean free path of the photons is much longer than the maximum range of the secondary electrons, a good approximation is possible.

With such a chamber, $P_{\mathrm{KA,o}}$ is obtained from equation (1) as

$$P_{\mathrm{KA,o}} = Q_{\mathrm{KAP}} \frac{W}{eh\rho_{\mathrm{air}}}, \tag{3}$$

where Q_{KAP} is the charge collected in the KAP-meter, W is the mean energy imparted per ion pair formed, e is the charge of an electron, ρ_{air} is the density of air and h is the total thickness of the air cavity. The calibration coefficient is then

$$k = \frac{W}{eh\rho_{\mathrm{air}}}. \tag{4}$$

Note that, defined in this way, the calibration coefficient is a constant independent of the x-ray spectrum.

4.2.2. The real KAP-meter

A KAP-meter usually consists of three plastic plates, typically PMMA or similar material of thickness 1-2 mm, to a total thickness of 4-6 mm. The plates are covered with a thin conductive coating, typically made of indium oxide doped with tin (In_2O_3:Sn) due to its transparency to light. The total thickness of the air layers (sensitive layers) in a modern KAP-meter is about 12-13 mm. The use of graphite coated KAP-meters have also been reported (Carlsson 1965a, Bednarek and Rudin 2000). The signal from these KAP-meters has a smaller energy dependence than that from indium oxide coated KAP-meters but, due to the graphite, the chambers are not transparent to light which is a drawback in overcouch installations where light is used to correctly position the x-ray beam at the patient. On the other hand, the less pronounced dependence of graphite-coated KAP-meters on the energy spectrum is an advantage in undercouch installations where light is not used to position the beam.

Photons incident on the KAP-meter will be attenuated in its walls, to an extent increasing with increasing angle of incidence and with decreasing photon energy. Further,

the conducting layer with an atomic composition deviating from that of air will cause a state of non charged particle equilibrium in the sensitive air volume.

In order to analyze the effects of photon attenuation and the non-air equivalence of the coating material on the calibration coefficient, k may be written:

$$k = \frac{P_{\mathrm{KA},r}}{Q_{\mathrm{KAP}}} = \frac{P_{\mathrm{KA},r}}{P_{\mathrm{KA,o}}} \frac{P_{\mathrm{KA,o}}}{P_{\mathrm{KA,i}}} \frac{P_{\mathrm{KA,i}}}{P^{\mathrm{p}}_{\mathrm{KA,i}}} \frac{P^{\mathrm{p}}_{\mathrm{KA,i}}}{A_{\mathrm{s}} \overline{D}_{\mathrm{air}}} \frac{W}{eh\rho_{\mathrm{air}}}. \qquad (5)$$

Here, $P_{\mathrm{KA},r}$, $P_{\mathrm{KA,o}}$, $P_{\mathrm{KA,i}}$ are the air kerma area products corresponding respectively to a reference plane, the KAP-meter exit and entrance planes (indexes "i" and "o" stands for "in" and "out"). $P^{\mathrm{p}}_{\mathrm{KA,i}}$ is the air kerma integrated over the entrance plane of the KAP-meter when only primary photons are considered. $\overline{D}_{\mathrm{air}}$ is the mean absorbed dose in the sensitive air volume and A_{s} is the area of the sensitive volume of the KAP-meter. The first two ratios show how P_{KA} changes between different reference planes. For example, choosing the patient plane as the reference plane, the first ratio ($P_{\mathrm{KA},r}/P_{\mathrm{KA,o}}$) shows how the value of P_{KA} differs between those two planes. The third ratio, $P_{\mathrm{KA,i}} \big/ P^{\mathrm{p}}_{\mathrm{KA,i}}$, quantifies the amount of backscatter while the fourth ratio, $P^{\mathrm{p}}_{\mathrm{KA,i}} \big/ (A_{\mathrm{s}} \overline{D}_{\mathrm{air}})$, quantifies the effect of lacking charged particle equilibrium in the air volume, and attenuation and scatter in the KAP-meter walls. The energy dependence of $P^{\mathrm{p}}_{\mathrm{KA,i}} \big/ (A_{\mathrm{s}} \overline{D}_{\mathrm{air}})$ produces considerable energy dependence in the calibration coefficient $P_{\mathrm{KA,o}}/Q_{\mathrm{KAP}}$. The last factor in equation (5) is the energy independent factor $\frac{W}{eh\rho_{\mathrm{air}}}$ (see equation (4)). The different factors can be studied using Monte Carlo simulations. Results of such simulations are discussed below (section 6.4) and presented in Paper IV.

5. Calibration procedures

In this section, three different calibration methods (methods 1, 2, and 3), applicable in overcouch geometries, are described. The drawbacks and advantages of the different methods are discussed. Calibration coefficients, k, derived using the different methods are denoted k_1, k_2, and k_3 respectively. Two sections deal with comparisons between calibration coefficients derived using different calibration methods. At under couch installations, where the couch and often a cushion are positioned between the KAP-meter and the patient, special considerations have to be made. Finally, two different approaches for deriving a calibration coefficient at undercouch installations are discussed

5.1. Method 1, using a nominal beam area

In practice, this calibration method is performed in many different ways. In principle P_{KA} is approximated as the product of $K_{c,air}$ and the nominal beam area A_{nom} in the patient plane ($P_{KA} \approx P_{KA,Anom}$ = the P_{KA} within A_{nom} in the patient plane, see Figure 1). $K_{c,air}$ is measured at the intersection of the central axis of the beam with the patient plane ($K_{c,air,centre}$). The corresponding calibration coefficient is

$$k_1 = \frac{K_{c,air,centre} A_{nom}}{Q_{KAP}} \qquad (6)$$

There are three different methods for estimating A_{nom}. The first two have been used in this work. The third method, described by Hansson (2006), shows how A_{nom} can be estimated using a digital x-ray equipment but has not been used here.

1. An extra collimator with a well-known aperture and the square law are used to determine $A_{nom} = A_{sq.law}$ at any distance from the focal spot (Carlsson 1996), cf. Figure 5.
2. An x-ray film (placed in a standard screen cassette) is positioned perpendicular to the beam axis and the beam area $A_{nom} = A_{film}$ is estimated from the size of the region with at least 50% of the maximum blackening (Shrimpton and Wall 1982). In IEC (1977) it is recommended that the x-ray film is exposed without intensifying screens and has an optical density of not more than 0.5.
3. This area estimation method is applicable when a computed radiography (CR-) system is used. Because of the non-linearity of the pixel values, the special procedure described below is performed (the raw, linear image 'for processing' is often not available to the user). An image (CR) plate is exposed (Image 1) to within the dynamic range of the detector. If available, the CR system with the smallest pixel

pitch (~ 100 μm) is selected. The image plate is then moved slightly perpendicular to the central axis and another exposure is made on it (Image 2) beside the first (the images must not overlap) using twice the mAs-value compared to the first. (The linearity of the indicated mAs-values of the x-ray generator should be carefully checked in advance.) The image plate is then read out and exported to the PACS. The images of the same beam area are now both visible beside each other on the viewing station, the only difference being that Image 2 was acquired using twice as many photons as Image 1. The "window width" is set at the smallest possible value (preferably 1). Then, increase the value of the "window level" position until Image 1 totally disappears. The visible boundary of Image 2 now indicates 50% of the maximum value of $K_{c,air}$ corresponding to A_{nom}. The area is estimated using the software tools for measuring distances or areas. The zoom-function should be maximized while measuring the distances. Care should be taken as to which plane the software tools are calibrated in. $K_{c,air,centre}$ and A_{nom} must be determined in the same plane. If it is impossible (due to practical reasons) to measure both $K_{c,air,centre}$ and A_{nom} in the same plane, one of them may be transformed by calculations to the other plane. A_{nom} derived this way may differ from A_{film} due to the non-linearity of the x-ray film.

The corresponding calibration coefficients (for the first two area estimation methods) are given by

$$k_{1,\mathrm{sq.law}} = \frac{K_{\mathrm{c,air,centre}} A_{\mathrm{sq.law}}}{Q_{\mathrm{KAP}}}, \tag{7}$$

$$k_{1,\mathrm{film}} = \frac{K_{\mathrm{c,air,centre}} A_{\mathrm{film}}}{Q_{\mathrm{KAP}}}. \tag{8}$$

Using this calibration method, the extra-focal radiation passing outside the nominal beam area is excluded while, due to the heel effect, the product of $K_{c,air,centre}$ and A_{nom} usually overestimates $P_{KA,Anom}$ (the air kerma integrated over A_{nom}, see Figure 1). The value of k_1 depends on the geometry of the calibration set-up and can vary substantially depending on the amount of extra-focal radiation and the distribution of $K_{c,air}$ within A_{nom} at the actual x-ray installation. In order to get an improved estimate of $P_{KA,Anom}$, some practitioners make additional measurements to get a better approximation of the mean $K_{c,air}$ within A_{nom}.

At the Primary standard laboratory PTB in Braunschweig, Germany, a special calibration geometry has been constructed which minimize the influence from both extra-

focal radiation and the heel effect by using a small beam area (5x5 or 2x2 cm^2 at 100 cm from the focal spot) defined by a collimator. The collimator and the plane of $K_{c,air}$ measurements are positioned at about 95 and 100 cm, respectively from the focal spot (Figure 2). After removing the KAP-meter, $K_{c,air}$ is measured at the reference plane (in the centre of the KAP-meter) using a free-air chamber. The calibration coefficient is then calculated using equation (7). Calibrated in this way, the KAP-meter will measure P_{KA} at the tube side of the KAP-meter in the absence of the KAP-meter (i. e. photons back scattered from the KAP-meter are not included in the measured P_{KA}). In what follows below, a KAP-meter calibrated this way is called a "Master KAP-meter" to distinguish it from KAP-meters used for clinical measurements which are calibrated to indicate the P_{KA} on the patient side of the KAP-meter. A Master KAP-meter is not the best choice for use in patient measurements since the measured P_{KA} must be corrected for the attenuation and scatter in the KAP-meter to give P_{KA} on the patient side. On the other hand, it is well suited for calibrating clinical KAP-meters, see section 5.3. PTB reports a relative expanded uncertainty in the calibration coefficient of 1.1-1.3% (coverage factor 2). Thus a calibration according to method 1 can be very accurate if rigorously performed.

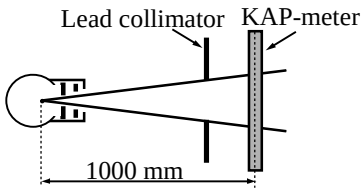

Figure 2. Schematic view of the experimental set-up for the calibration of a Master KAP-meter using a collimator with a well-defined aperture to determine the beam area. The KAP-meter signal is related to the air kerma area product of the incident photons as measured at a standard laboratory using a free-air chamber (from Paper V).

5.1.1. Determination of A_{film}

The 50% isodensity curve on the x-ray film is preferably derived using a microdensitometer or a scanner. In practice, however, the areas are often measured visually using a ruler. Consequently, the result of the measurement depends on the observer. In both cases, the results also depend on the maximum optical densities of the films. This was investigated in Paper III.

5.1.2. Dependence of A_{film} on optical density

Using a focus-film distance of 100 cm and tube voltage 70 kV, the dependence of A_{film} on optical density was examined using several x-ray films exposed so as to give maximum optical densities ranging from 0.35 to 3.5,. The films were scanned in a Vidar x-ray film scanner (VXR-12, Vidar Systems Corporation, Herndon, VA. U.S.A.). Automatic tracking and determination of areas within isodensity curves were performed using a computer programme (Poseidon 2.0 pre-release, Precitron AB, Uppsala, Sweden) to determine the areas within 10, 50 and 70% of the maximum density. The results are shown in figure 4. Films were also exposed to maximum optical densities below 0.5 (as recommended in (IEC 1977), but the programme could not accurately perform automatic tracking of isodensity curves at such low densities. Beam areas on the same films (circles (○) in Figure 3) and on films exposed at another x-ray stand (squares (□)) were also determined visually.

The values of estimated beam areas increase with increasing optical density and depend on the isodensity level used for its definition (Figure 3). However, the response of the eye does not follow that of the film scanner. At maximum densities above 1.5 ODU the visually estimated area is 5% larger than that determined by scanning and the deviation increases further with increasing maximum optical density. It should be noted that the results, though qualitatively valid, depend on the particular x-ray stand and its collimation as demonstrated by the results for the second set of films (□). In the latter case, the estimated beam area increases by less than 2% for maximum optical densities between 0.44 and 1.7 ODU (compared to 10% for the first set).

At optical densities above 3.5 ODU, the film is saturated at the centre and the program tracks extra-focal radiation outside the region hit by radiation from the focus, resulting in increased estimates of the area.

5.1.3. Interobserver variations in estimates of A_{film}

The spread in area estimation among six independent observers is shown in Figure 4. Six x-ray films, irradiated with different beam areas at an x-ray tube with an old lead glass collimator, were used. For each film, the individual estimations were divided by the mean of the estimated areas. As expected, the variation is greater at small mean areas, since the uncertainty in the estimation of the side lengths is relatively greater at small areas. For areas of about 100 cm^2 (the size of beam area recommended by NRPB (1992)), the variation was 7% at the 95% confidence level. The large spread of values shown in Figure 4 is due to the blurred beam edges caused by the lead glass collimator and extra-focal radiation. The optical density of the films used in Figure 4 (1.3 ODU) is not optimal and the corresponding variation was only 3% for films exposed to densities below 0.5 ODU (area 100 cm^2). At these low densities, the x-ray film characteristics suppress the blackening outside the area of focal radiation.

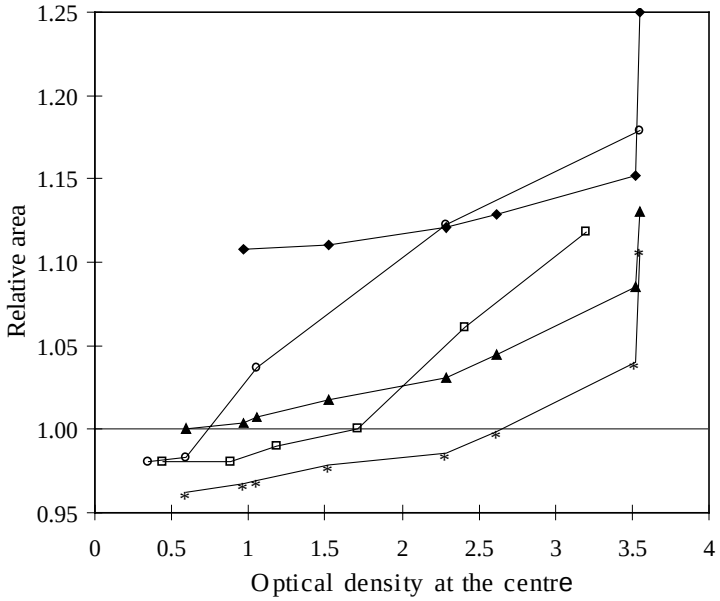

Figure 3. Estimated beam area as a function of the optical density at the centre of the x-ray film. Two methods were used, film scanning and visual inspection. Values are normalized to that (87.7 cm^2) obtained using film scanning and the 50% isodensity curve (▲) at 0.59 ODU. The areas within 10% (◆) and 70% (*) isodensity curves were also calculated. Visual estimations were made (within the 50% isodensity level) for two sets of films, The same as that used for the film scanning (○) and films exposed at another x-ray stand (□) normalized to the values of the former at 0.44 ODU (from Paper III).

Films were also exposed at maximum optical densities 0.5 and 1.3 ODU to a beam of area 300 cm^2 at an x-ray tube with a modern collimator giving sharper beam edges. The variations among ten different observers were only 1% and 1.3% (at the 95% confidence level) for the 0.5 and 1.3 optical densities, respectively.

As demonstrated above the uncertainty in estimating A_{film} depends on optical density, beam area, type of beam collimation and method used (scanning or visual inspection). According to NRPB (1992), beam areas should be determined with an uncertainty of no more than 5% at the 95% confidence level, for a beam area of 10x10 cm^2. To comply with this requirement, low optical densities (≤0.5 ODU) as recommended in IEC (1977) must be used. According to IEC, the film should also be exposed without intensifying screens which would probably decrease the uncertainty in the beam area estimation due to reduced blurring of the beam edges. In practice, however, it is common and convenient to expose the films in a standard screen cassette as described by Shrimpton and Wall (1982). However, using intensifying screens the desired low optical densities may not be possible to achieve at some x-ray installations without using additional filtration.

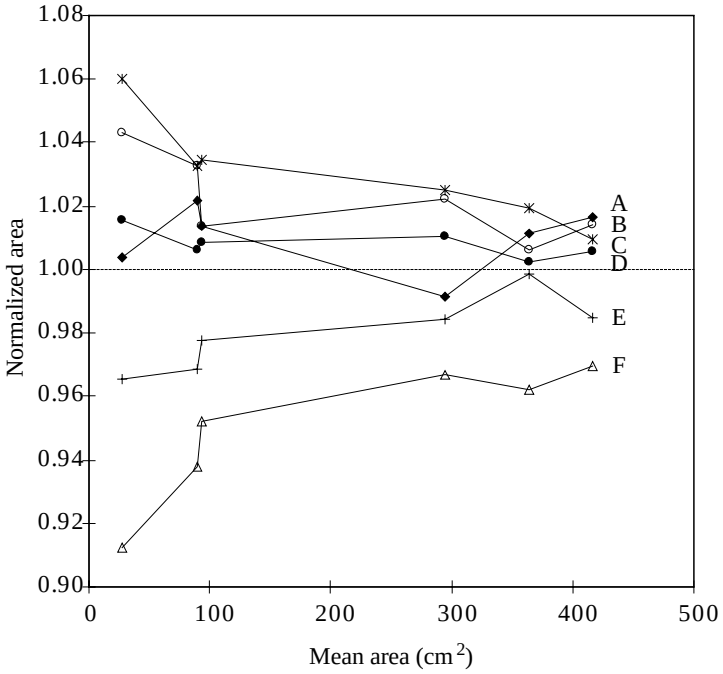

Figure 4. Visual estimates of beam area made by six independent observers (indicated by letters A-F in the figure). The values for each film were normalized to the means of the area estimated by the six observers and plotted as a function of mean area. The films were exposed to density 1.3 ODU at an x-ray tube with an old lead glass collimator, giving unsharp beam edges.

5.2. Method 2, estimate from integration

This calibration method was developed and described in Paper I. It has not been described elsewhere and therefore a rather comprehensive description of the method is presented in the following subsections. See Paper I for more details.

5.2.1. Equipment

Two types of KAP-meters were used: KM1 (type 57523(B), PTW-Frieburg), consists of three plastic plates coated with a conducting layer of indium oxide doped with tin (In_2O_3:Sn). KM2 (Carlsson 1965, not commercially available) consists of three plastic plates coated with a thin conducting carbon layer. A spherical (3.7 cm^3) ionisation chamber (the reference chamber) with a calibration traceable to the primary standard at BIPM (Bureau International des Poids et Mesures) was used for measurements of the air collision kerma ($K_{c,air}$). Dosimeters of thermoluminescent LiF (LiF:Mg, Ti) of diameters 4.5 mm and thickness 0.9 mm were read out in a Harshaw TLD System. Irradiations were performed

using a Siemens x-ray tube (Bi 200/20/50S), with a 12-pulse generator Triplex Optimatic 1023 (Siemens).

5.2.2. The calibration procedure

This calibration implies determination of the P_{KA}-value, $\int_A K_{c,air} dA$, for an integration area A that extends beyond the nominal beam area in order to arrive at a geometry independent calibration coefficient. The $\int_A K_{c,air} dA$ was achieved in two steps. First, the normalised integral $\int_A \frac{K_{c,air}}{K_{c,air,centre}} dA$ was determined using the TL-dosimeters. Next, the air collision kerma at the centre of the beam, $K_{c,air,centre}$, was measured with the reference chamber. The product of these values gave $\int_A K_{c,air} dA$.

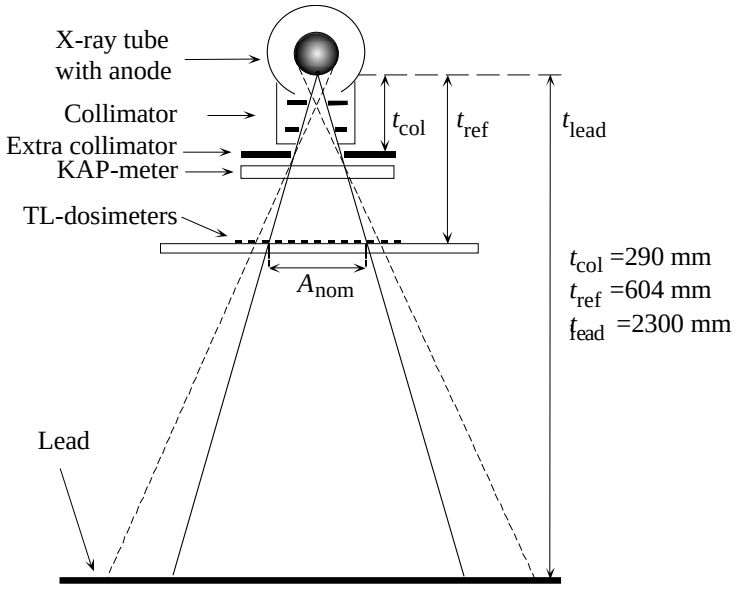

Figure 5. Experimental set-up for determination of air collision kerma integrated over beam area A, $\int_A K_{c,air} dA$. A 3 mm thick square lead collimator (of area 24.8 cm^2) was placed close to the KAP-meter to define the beam area. Thermoluminescent dosimeters were placed on a 10 mm thick sheet of expanded cellular polystyrene perpendicular to the beam axis. A 5 mm thick lead plate prevented backscatter from the floor. To determine $K_{c,air}$ on the beam axis, the polystyrene sheet was replaced by a spherical (3.7 cm^3) ionisation chamber centred on the beam axis. The solid and dotted lines indicate focal and extra-focal radiations, respectively. The nominal beam area, A_{nom} is defined by the primary beam (Figure 1 in Paper I).

The normalised integral $\int_A \frac{K_{c,air}}{K_{c,air,centre}} dA$ was determined with TL-dosimeters (Figure 5) positioned over an area (A) large enough to register not only the focal but also the extra-focal radiation passing through the KAP-meter and contributing to its signal Q_{KAP}.

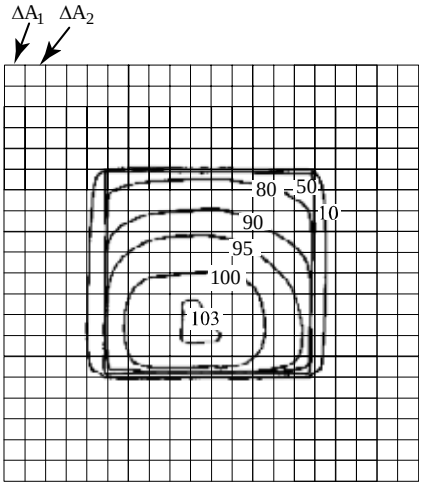

Figure 6. Isodensity curves (set to 100 at the centre) on an x-ray film exposed perpendicularly to the beam axis, 60 cm from the focal spot and at a tube voltage of 150 kV. Squares (ΔA_i, 1x1 cm^2) at the centre of which TL-dosimeters were positioned are indicated.

One dosimeter was placed at the centre of each one of 400 1x1 cm^2 area elements covering an area (Figure 6) extending beyond A_{nom} and the normalized integral was determined as

$$\int_A \frac{K_{c,air}}{K_{c,air,centre}} dA \approx \sum_i \left(\Delta A_i \frac{M_i}{M_{centre}} \right) \qquad (9)$$

Here, M_i is the signal from TL-dosimeter i (corrected for background and individual sensitivity) in area element ΔA_i and M_{centre} is the mean signal from nine TL-dosimeters at the centre of the beam. In area elements with steep $K_{c,air}$-gradients, as at the edges of the nominal beam area, A_{nom} (Figure 5), additional measurements were performed to correct the measured signals M_i to correspond to the average $K_{c,air}$ in ΔA_i using both TL-dosimeters and x-ray films.

Values of the normalised integral are presented in Table 1. For comparison, integration was restricted to A_{nom} (A_{nom}=107.6 cm^2 at the actual distance (604 mm) from the focal spot). Since the quotient $K_{c,air}/K_{c,air,centre}$ is dimensionless, the integral will be in units of area and

can be directly compared with A_{nom}. Since the integral restricted to A_{nom} $\left(\int_{A_{\mathrm{nom}}} \frac{K_{\mathrm{c,air}}}{K_{\mathrm{c,air,centre}}} \mathrm{d}A \right)$ is less than A_{nom}, the quotient $K_{\mathrm{c,air}}/K_{\mathrm{c,air,centre}}$ is, on the average, less than unity (due to the heel effect), implying that the product $K_{\mathrm{c,air,centre}}A_{\mathrm{nom}}$ is an overestimate of $\int_{A_{\mathrm{nom}}} K_{\mathrm{c,air}} \mathrm{d}A$. Even so, it underestimates the integral over the total area A since the extra-focal radiation passing outside A_{nom} is excluded. The discrepancy between $K_{\mathrm{c,air,centre}}A_{\mathrm{nom}}$ and $\int_A K_{\mathrm{c,air}} \mathrm{d}A$ depends on the relative influence of two counteracting effects; the heel effect and the escape of extra-focal radiation from A_{nom}.

The contribution to the integral $\int_A K_{\mathrm{c,air}} \mathrm{d}A$ from regions outside A_{nom} is about 4%. For other x-ray tubes, generator settings, beam areas and distances from the focal spot, the contribution from extra-focal radiation may be quite different.

Table 1. Values of the normalised integral (see equation (9)) $\int_A \frac{K_{\mathrm{c,air}}}{K_{\mathrm{c,air,centre}}} \mathrm{d}A$ at tube voltages of 40, 70 and 150 kV. For the irradiation geometry see Figure 5. Partial integrals over and outside the nominal beam area (A_{nom} = 107.6 cm^2) are also shown. The error intervals indicate one standard uncertainty in the measured values (ISO 1993) (from Paper I).

	Integrals over different areas (cm^2)		
Tube voltage (kV)	$\int_A \frac{K_{\mathrm{c,air}}}{K_{\mathrm{c,air,centre}}} \mathrm{d}A$	$\int_{A_{\mathrm{nom}}} \frac{K_{\mathrm{c,air}}}{K_{\mathrm{c,air,centre}}} \mathrm{d}A$	$\int_{A>A_{\mathrm{nom}}} \frac{K_{\mathrm{c,air}}}{K_{\mathrm{c,air,centre}}} \mathrm{d}A$
40	108.8 ± 1.4	104.9	3.9
70	108.7 ± 1.4	104.0	4.7
150	110.3 ± 1.4	105.7	4.6

5.2.3. The calibration coefficient k_2

Total P_{KA} -values were determined as

$$P_{\mathrm{KA}} = K_{\mathrm{c,air,centre}} \int_A \frac{K_{c,air}}{K_{c,air,centre}} dA \approx$$
$$\approx K_{\mathrm{c,air,centre}} \sum_i \left(\Delta A_i \frac{M_i}{M_{\mathrm{centre}}} \right) \qquad (10)$$

$K_{c,air,centre}$ was measured with a small calibrated ionization chamber replacing the TL-dosimeters and polystyrene sheet, cf. Figure 5. The calibration coefficients were obtained using equation (2). The calibration coefficients for the two KAP-meters KM1 and KM2 are shown in Figure 7.

Due to the different atomic numbers of their conducting layers, KM1 is more sensitive than KM2. The layer in KM1 contains indium which, besides its higher sensitivity, also results in a larger energy dependence compared to the graphite-coated KM2, see section 6.

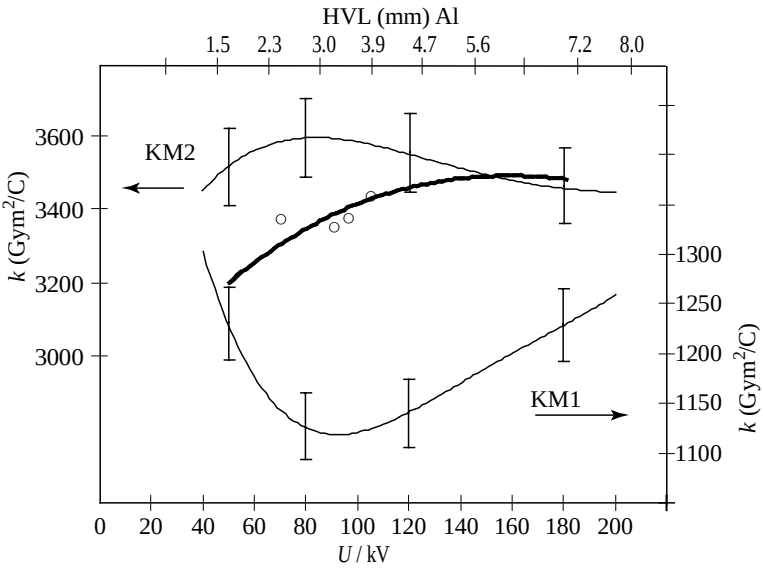

Figure 7. Calibration coefficients k for two KAP-meters at NTP (20°C and 101.325 kPa). Lower curve: KM1 (scale on right ordinate); upper curve: KM 2 (scale on left ordinate). The thick line (calibration method 1, $k_{1,sq.law}$) and the symbols, o, (a calibration method that took into account the variation of $K_{c,air}$ over the beam area) were taken from Carlsson 1965 (KM2). The error bars indicate ± two combined standard uncertainties (3%), and are the same for both chambers. The main contribution to the uncertainties is due to parameters (e.g., *RAK*) that are essentially energy independent (see Table 1 and Table 4)

The characteristics of the KAP-meters are obviously strongly dependent on the atomic composition and thickness of the coating layer. Non-uniformity of the conducting layer on the KAP-meter electrode could be crucial to its performance since, in this case, the proportionality between P_{KA} and the charge Q_{KAP} would not be independent of the beam area. Measurements of the response on different parts on the surface of KM1 (figure 4 in Paper I) show that it is fairly constant and that the sensitivity variations noted will have only a minor impact on the proportionality between P_{KA} and Q_{KAP}.

The proportionality will be at risk if recombination occurs in the KAP-meter. Recombination was, however, found to be negligible at the normal polarizing voltage (+500 V) and for $K_{c,air}$ -rates up to 400 mGy s^{-1}.

5.3. Method 3, using a Master KAP-meter

A calibration method which is easy to perform is to measure P_{KA} with a Master KAP-meter (calibrated at a primary standard laboratory as described in section 5.1.). A typical geometry is shown in Figure 8.

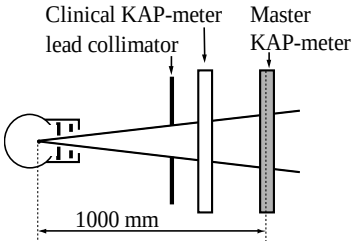

Figure 8. Calibration of a clinical KAP-meter using a Master KAP-meter.

The calibration coefficient, k_3, for the clinical KAP-meter is calculated as

$$k_3 = \frac{Q_{KAP,M}\, k_M}{Q_{KAP}}, \qquad (11)$$

where index "M" stands for the Master KAP-meter. If the distance between the Master and the clinical KAP-meter is not too large, so that practically all the radiation transmitted through the clinical KAP-meter impinges on the Master KAP-meter, $Q_{KAP,M}\, k_M$ essentially measures $P_{KA,o}$, provided the response to the obliquely incident scattered photons from the clinical KAP-meter does not deviate too much from that of the (perpendicularly incident) primary photons.

Placing the KAP-meters close to each other may introduce errors due to photon scattering between them. The distance between the lead collimator and the clinical KAP-meter is of minor importance since scatter from the collimator edges is negligible (Grindborg 2006). The value of k_M should be valid for the x-ray spectrum incident on the Master KAP-meter, i.e. the effect of the filtration of the clinical KAP-meter on the energy spectrum should be taken into account. The filtration of a typical KAP-meter increases the HVL by about 5-7% for the x-ray spectra RQR2 and RQR10 (Grindborg 2006). When calibrations of clinical KAP-meters are performed using energy spectra that differ considerably from those used at the standard laboratory for calibrating the Master KAP-

meter, the appropriate choice of k_M is crucial. Even though k_M is available as a function of tube voltage, mean energy (with respect to $K_{c,air}$) and HVL the correct choice of k_M in equation (11) for the clinical spectra is difficult.

5.4. Comparisons of calibration methods 1 and 2

5.4.1. Calibrations according to method 1 in an experimental laboratory

The calibration coefficients determined with method 1 (k_1) depend on the experimental set-up. The uncertainties thereby introduced are demonstrated in the following.

$A_{\text{square law}}$ was determined using three extra collimators (Figure 5) with square apertures of areas 5, 25 and 100 cm^2. $K_{c,air,centre}$ was measured and the corresponding values of $A_{\text{square law}}$ calculated at distances from the focal spot ranging from 50 to 160 cm.

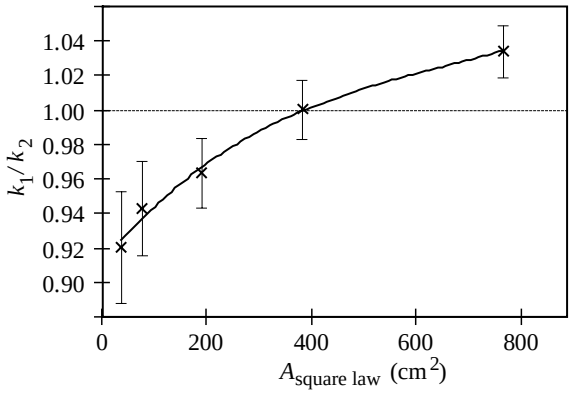

Figure 9. Quotients $k_{1,\,\text{sq.law}}/k_2$ (KM1) of calibration coefficients obtained using method 1 and the method 2 as a function of $A_{\text{square law}}$ (distance from the source 80 cm, tube voltage 70 kV). Five opening apertures of the extra collimators (of areas 5, 10, 25, 50 and 100 cm^2) give values of $A_{\text{square law}}$ of 38, 76, 190, 380 and 761 cm^2 respectively. Error bars indicate ±two standard deviations of the estimated stochastic errors (see Paper I for an explanation).

The position of the focal spot needs to be accurately determined since values of $A_{\text{square law}}$ are calculated using the inverse square law. This position was determined with a standard triangulation method using the x-ray images of two needles with known distances between them and between the needles and the film. A_{film} was determined using the 50% isodensity curve measured either with a microdensitometer, or estimated visually, both with and without extra collimators.

The quotients between the simplified calibration coefficients $k_{1,i}$ (where i = square law or i = film) and k_2 were investigated as a function of beam area and distance from the focal

spot. The results are shown in Figure 9 and Figure 10. Since k_2 is independent of geometry, the variations of $k_{1,i}/k_2$ with beam area and focal distance shown in Figure 10 and Figure 11 are due to the dependence of $k_{1,i}$ on these parameters.

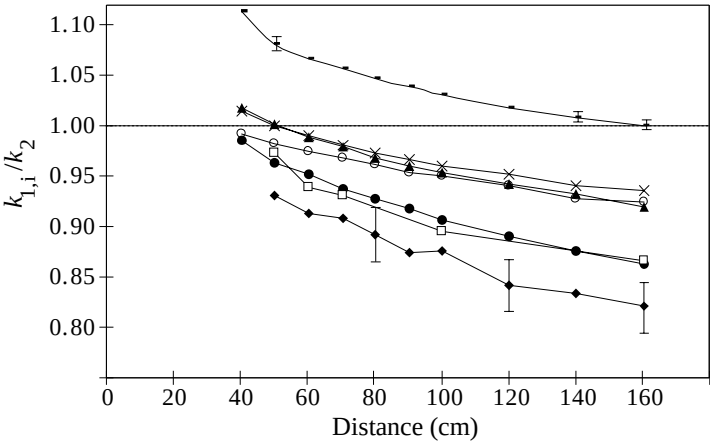

Figure 10. Quotient $k_{1,i}/k_2$ (KM1) of calibration coefficients obtained using calibration method 1 with two different methods for determining the beam area (i = sq.law, film) and calibration method 2 as a function of distance from the source of the reference chamber. The size of the extra collimator and the tube voltage are parameters. Method 1, $A_{\text{nom}} = A_{\text{square law}}$, with extra collimators of area: – 100 cm^2 (40 kV), ▲ 25 cm^2 (40 kV), ● 5 cm^2 (40 kV), × 25 cm^2 (70 kV), ○ 25 cm^2 (150 kV). Method 1, $A_{\text{nom}} = A_{\text{film}}$: □ no extra collimator (40 kV), ◆ with a 5 cm^2 extra collimator (40 kV). Without an extra collimator, A_{film} corresponds to a virtual extra collimator of area 9.4 cm^2 as estimated from the value of A_{film} and the square law (cf. Figure 5). The error bars indicate ±two standard deviations of the estimated stochastic errors (see explanations in Paper I).

The ratio $k_{1,i}/k_2$ can be written:

$$\frac{k_{1,i}}{k_2} = \frac{A_{\text{nom}} K_{\text{c,air,centre}}}{\int_A K_{\text{c,air}} \text{dA}}, \qquad i\text{= sq.law, film.} \tag{12}$$

From Figure 6, it is seen that due to the heel effect, $K_{\text{c,air,centre}}$ multiplied with the nominal beam area (A_{film}) can overestimate $\int_A K_{\text{c,air}} \text{d}A$ at large beam areas resulting in values of $k_{1,i}/k_2$ greater than one. For smaller beam areas, especially at large distances from the source, $k_{1,i}/k_2$ is smaller than one. The reason for this is not obvious from Figure 6. However, in figure 9, Paper I, in which profiles of the beam at different distances are plotted, the escape of extra-focal radiation to outside A_{nom} at large distances is demonstrated. The influence of the latter on the measured value of $K_{\text{c,air,centre}}$ is shown in figure 6, Paper I, and explains why

$K_{c,air,centre}$ (at a given distance from the focus) decreases when the collimator opening is decreased.

Even with identical energy spectra, the dependencies on beam inhomogeneities (heel effect and extra-focal radiation) demonstrated above, may cause the calibration coefficients k_1 to vary appreciably between different x-ray tubes. This may be the reason for recommending that calibrations be performed at the particular x-ray stand where the KAP-meter is to be used and in a geometry similar to that used in the examinations (IEC 1977, NRPB 1992, ISO 1993). As was pointed out in section 5.2.3. this is not necessary using a KAP-meter which has been calibrated according to calibration methods 2 and 3.

The influence of the extra-focal radiation normally counteracts the influence from the heel effect. Fort a certain beam area, distance from focus and tube voltage they will balance each other so that the calibration coefficient k_1 coincides with k_2. Carlsson (1965, 1996) performed calibration according to both method 1 and one similar to method 2. His choice of beam area and distance from the source may explain the agreement obtained between the two calibrations coefficients (cf. Figure 7). The influence of the extra-focal radiation and the dependence on beam geometry demonstrated here were not noted (Carlsson 1996).

5.4.2. Calibrations according to method 1 at clinical x-ray installations

Simplified calibrations according to method 1 (equation (6)) are performed all over the world by hospital physicists. Even though the variations in beam area or distance from the focal spot, etc., are probably much less than those tested above, other sources of errors could be present. For example, the HVL of the radiation (beam quality) may not be known accurately (resulting in a wrong choice of calibration coefficient for the reference chamber), the couch table may not be removable (resulting in a backscatter contribution to $K_{c,air,centre}$), different sizes of reference chamber may be used, varying relative amounts of extra-focal radiation may be present, the optical densities of the film used for determining A_{film} may vary etc. Calibration coefficients (k_1) obtained from participants in a workshop on KAP-meter calibrations (see Paper III) were therefore compared with the coefficients derived with calibration method 2.

Several hospital physicists in Sweden declared in our contacts with them that they would like to meet and compare KAP-meter calibrations. The Radiation Physics Department in Linköping therefore arranged the workshop cited above. Participants brought their own KAP-meters and were asked to bring (if available) their own calibration coefficients. The KAP-meters were then calibrated in terms of the calibration method 2 by comparing their signals with that from a KAP-meter previously calibrated according to method 2. A small ionization chamber was used for output normalisation. The tube voltages ranged from 50 to 140 kV.

In order to get more data on calibration coefficients using method 1 at different x-ray installations, such calibrations were also performed according to normal practice at clinical x-ray installations in both Linköping and Växjö. Two cylindrical reference chambers with volumes of 6 and 30 cm^3 with calibrations traceable to BIPM were used. The focus-reference chamber distance was usually 100 cm. In some cases, $K_{c,air,centre}$ measurements had to be made in front of the patient couch (with possibly some back scatter contributions to the readings). Values of A_{film} were estimated visually using a ruler and, due to variations in the procedures used by different practitioners, the optical densities at the centres of the films ranged from 0.4 to 2.7. The factory calibrations of four KAP-meters (from two different manufacturers) were also included in the comparison (see Figure 11).

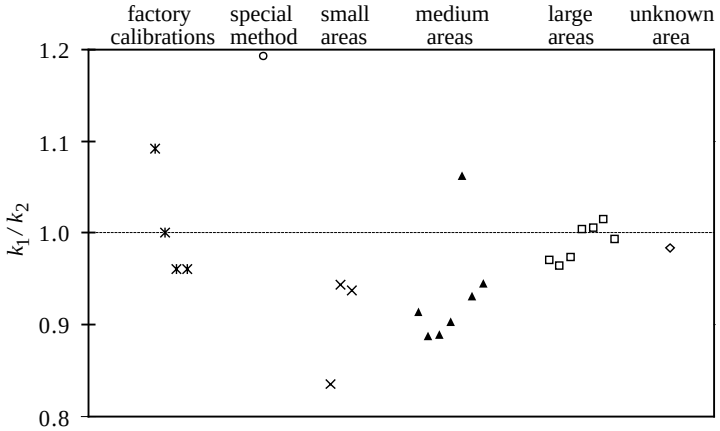

Figure 11. Quotients between calibration coefficients k_1 (obtained under different conditions and at different x-ray installations) and k_2. ∗: factory calibrations; ○: special method (see text); ×: small areas < 80 cm^2; ▲: medium areas 80-120 cm^2; □: large areas > 120 cm^2 (all areas were measured at the position of the reference chamber); ◊: beam area unknown. Tube voltage: 90-120 kV. (From Paper III).

Quotients less than one mean that $A_{film}K_{c,air,centre}$ underestimates $P_{KA,o}$ (cf. equation (12)) and imply that the escape of extra-focal radiation dominates over the counteracting heel effect. With no extra-focal radiation present, the $A_{film}K_{c,air,centre}$ usually overestimates $P_{KA,o}$ due to the heel effect.

From Figure 11, it can be seen that in general, large areas give quotients closer to unity than small areas in accordance with the results of Paper I. The large number of quotients less than one implies that, in most cases, the influence of the escape of extra-focal radiation is the dominating effect. For the x-ray installations used, this is the case even at beam areas between 200 and 350 cm^2 (the three squares to the left in Figure 11). The beam area has to be ≥ 400 cm^2 for the escape of extra-focal radiation to be balanced by the influence of the

heel effect (the four squares to the right in Figure 11). This is in accordance with the results in Figure 10 (for distances from the focus between 90 and 100 cm).

It must be stressed that the influences of the heel effect and of extra-focal radiation depend on the type of x-ray tube, its beam collimation and filtration, age, type of generator etc. The fifth triangle from the left in Figure 11 was obtained using a rather small beam of area 96 cm^2 but still yields a high value of 1.06 for the quotient k_1/k_2. This could be a result of good collimation close to the focal spot (reducing the influence of the extra-focal radiation) and/or a small anode angle giving a large heel effect. It is in this case, however, most likely to be due to the high optical density (2.7 ODU) used in this determination of A_{film}. The results in Figure 3 indicate that this may cause an overestimate of A_{film} by as much as 8-14%.

The value marked "Special Method" ($k = k_s$) in Figure 11 was determined using yet another calibration method performed as follows: The KAP-meter was calibrated to measure $K_{c,air}$ when inserted in a beam covering the whole area of the KAP-meter and a kerma calibration coefficient (N_k) was assigned to the chamber. The effective area (A_{eff}) of the KAP-meter was then derived as follows: The KAP-meter was irradiated at its centre using a beam of known area A (smaller than that of the KAP-meter area) and the reading (R_A) was compared with that obtained when the KAP-meter was fully irradiated (R_{full}). The effective area was derived as

$$A_{eff} = A\frac{R_{full}}{R_A},$$

and the calibration coefficient k_s obtained as

$$k_s = N_k A_{eff}. \qquad (13)$$

The following comments may be made about this calibration method:

1. The kerma calibration coefficient N_k is defined to give the air kerma at the position of the chamber but without the chamber present. If no corrections are made for attenuation in the KAP-meter, the calibration coefficient k_s gives P_{KA} on the tube side of the KAP-meter. P_{KA} on the patient side may be determined by correcting the value of P_{KA} on the tube side with a factor accounting for attenuation and scatter in the KAP-meter. This could explain the major part of the deviation of k_s/k_2 from unity for this KAP-meter in Figure 11.
2. The values of k_1 (obtained with calibration method 1) are influenced by beam inhomogeneities. The same applies for values from calibrations according to

equation (13) which depend on the inhomogeneities in the beams used both for the N_k calibration and for determining A_{eff}.

3. In Figure 11, the tube voltage chosen for the intercomparison was selected to be between 90 and 120 kV to avoid the steep gradient in the calibration curve at lower tube voltages (see Figure 7). When compared at 50 kV, the ratio k_s/k_2 increased to 1.30. This cannot be explained by increased attenuation (in the KAP-meter) only but may be due to differences in the energy-dependence of the reference chambers used in the calibrations.

5.5. Comparisons of methods 1 and 3

Calibration method 3 can be considered as a method of determining $P_{KA,o}$ while method 1, applied as recommended by NRPB (1992), approximately determines $P_{KA,Anom}$ (i.e. the value of P_{KA} restricted to the nominal beam area, A_{nom}, in the patient plane). As demonstrated in the previous sections the value of k_1 depends on the x-ray installation and the calibration geometry while the value of k_3 is independent of the geometry and can be used at any x-ray installation. In section 6.2.1. Monte Carlo simulations to calculate the quotient of k_3 to k_1 are described. The quotient was found to be about 1.15 for the specific geometry simulated. The deviation between k_3 and k_1 is further discussed in section 6.4.4. Correlations to the radiation risk for the patient using different choices of P_{KA}, are further discussed in section 8.

5.6. Calibration at undercouch installations

At undercouch installations the deviation between $P_{KA,o}$ and $P_{KA,patient}$ (the air kerma at the patient entrance plane integrated over the area traversed by photons hitting the patient) is considerable due to the attenuation and scatter of photons in the couch. Here two methods for deriving a calibration coefficient $k_{patient}$ giving $P_{KA,patient}$ at under couch installations are proposed.

5.6.1. Correction of over-couch calibration coefficients

Calibration coefficients $k_3 = P_{KA,o}/Q_{KAP}$ derived at over couch installation are corrected for the effects of attenuation and scatter in the couch. The combined effect of scatter and attenuation could be measured simultaneously by putting an ionization chamber just above the couch, with and without the couch in position, Figure 12. Beams of clinical relevant areas and tube voltages should be used since the magnitude of the correction factor depends on beam area as well as on tube voltage. If the correction factor is measured in "narrow beam" geometry (as is usually recommended in attenuation measurements) and used to correct the calibration coefficient k_3, the $P_{KA,patient}$ will be underestimated. This underestimate is due to photons scattered from the couch that may reach the patient.

Carlsson (1965) measured calibration coefficients for both over- and under-couch installations for HVT (mm Al) ranging from 3 to 8 mm. The beam area was not specified. The quotient between over- and undercouch calibration coefficients varied between 1.28 (at HVT 3 mm) and 1.12 (at HVT 7 mm).

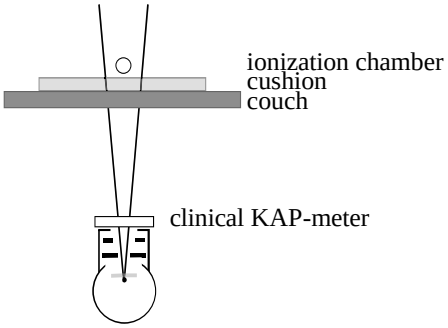

Figure 12. Geometry at under-couch calibrations.

A practical problem in measuring the attenuation in the couch at clinical installations may be that the couch cannot be removed from the beam. If, to solve this problem, measurements are performed just below the couch and corrected (using the inverse square law) to a point just above the couch, two additional possible errors are introduced:
a) Radiation back scattered, from the couch to the ionisation chamber below the couch, is included in the measurement (leading to a too high value of couch "attenuation").
b) Due to extra-focal radiation, the inverse square law may not apply, see Figure 10. Especially, if readings are corrected over a long distance to avoid problems with a) above, additional uncertainties of several percent may be introduced.

5.6.2. A new calibration coefficient derived using a Master KAP-meter

In IAEA (2006) a method (similar to calibration method 3, section 5.3) for using a Master KAP-meter to derive calibration coefficients at under-couch installations is described. In this method the Master KAP-meter is positioned on top of the couch and a beam of approximate area 100 mm x 100 mm at the position of the Master KAP-meter is used (the spherical ionization chamber in Figure 12 is replaced by a Master KAP-meter), see IAEA (2006) for more details.

To improve patient comfort, clinical x-ray examinations are often performed using an additional cushion. If this is done, this cushion should also be used in the calibration set-up. The influence of the couch and cushion on the HVL of the x-ray spectrum should be taken

into account when choosing the values of the calibration coefficient to be used for the Master KAP-meter.

A typical KAP-meter has a sensitive area of about 165 mm x 165 mm and there is only about 33 mm between the edges of the sensitive volume of the chamber and of the beam edge when the beam area recommended in IAEA (2006) is used. Correct positioning of the chamber at the centre of the beam is therefore important. Extra-focal radiation is distributed not only inside but (especially at long distances from the collimators) also outside the nominal beam area (Larsson *et al* 1996) and may even pass outside the sensitive volume of the Master KAP-meter. Prior to calibration, this should be checked with a film or other imaging device. To reduce the problem (in the calibration situation) of extra-focal radiation outside the sensitive volume the beam area and/or (if possible) the distance between the collimators and the Master KAP-meter could be reduced. If reduction of the distance is made, care should be taken so as the distance between the clinical KAP-meter and the couch does not become so small that back-scattered radiations from the couch to the clinical KAP-meter introduce uncertainties in the derived calibration coefficients. If the distance between the clinical KAP-meter and the couch is more than 30 cm the influence of back-scattered radiation is less than a few percent (Carlsson 1965a).

Questions have been raised as to whether Master KAP-meters calibrated according to e.g. the method used at PTB in Braunschweig, can correctly measure $P_{KA,i}$ when used in measurement set-ups (placed on top of the couch and cushion) so very different from the calibration geometry. The main concern is photons scattered from the couch which hit the Master KAP-meter at oblique incidence and hence may change the KAP-meter response (i.e. change the proportionality between Q_{KAP} and $P_{KA,i}$). In Paper IV,- calibration coefficients are derived for the exit plane of the KAP-meter ($k = P_{KA,o}/Q_{KAP}$) in two configurations. 1. With an additional filter (2 mm Al + 0.15 mm Cu) placed closely in front of the KAP-meter and 2. With the additional filter treated as an ideal non-scattering filter. The calibration coefficients derived for these two configurations show no or only small differences (within 3%, see Table 3) when the exit plane is used as the reference plane. Thus it is expected that the Master KAP-meter can measure the P_{KA} above the table at an under couch installation with only small additional errors (within 2%) as compared to the over couch situation. This requires the primary beam, any extra-focal radiation, and radiation scattered from the couch to be confined within the sensitive area of the KAP-meter.

6. Energy dependence of the KAP-meter calibration coefficient

The energy dependence of KAP-meter calibration coefficients is the variation of the calibration coefficient (k) with variations in photon energy and is often described in terms of the variation of response (calibration coefficient) on tube voltage and filtration or half value layer (HVL). Papers IV and V both deal with analyzing the energy dependence of the KAP-meter calibration coefficients which is large compared to those of ionization chambers used for measurements of $K_{c,air}$. The uncertainties in reported P_{KA}-values will increase due to the energy dependence, for example, when different energy spectra are used in calibration and in clinical measurements. Figure 13 shows the variation of the calibration coefficient for KM1 obtained using calibration method 1 (for incoming radiation) at PTB in Braunschweig (see section 5.1) . The coefficients are plotted for two different sets of reference radiation qualities (RQR and RQA). The RQR spectra are filtered with 2.5 mm Al while the RQA spectra are heavily filtered with Al of varying thickness (from 6.5 mm at 40 kV to 47.5 mm at 150 kV) yielding values of calibration coefficients, k_M, that differ by as much as 30% for the same mean energy and HVL. In the clinic, filtrations as low as 2.5 mm Al are seldom used. It is supposed that x-ray spectra common in the clinic lie between the RQR and RQA spectra and consequently, curves of calibration coefficients are supposed to lie between the two calibration curves shown in Figure 13 for spectra common in the clinic.

The reasons for the energy dependence are analyzed in this section and different factors influencing it discussed. In short, all construction details of the KAP-meter which deviate from that of the ideal KAP-meter contribute to the observed energy dependence. In addition, the ideal KAP-meter calibration coefficient has also an energy dependence if $P_{KA} = P_{KA,Anom}$ and a filter is positioned close in front of the KAP-meter. In this case, the fractions of photons hitting A_{nom} (in the patient plane) will depend on the filtration and the tube voltage as will the calibration coefficient. If $P_{KA} = P_{KA,o}$ then the ideal KAP-meter calibration coefficient has no energy dependence, even if a filter is placed close in front of it.

Scatter (from the KAP-meter and filters), extra-focal radiation and the heel effect may influence the energy dependence to a degree which depends on the choice of calibration method, reference plane, and area of integration (discussed in Paper IV). This means that calibration coefficients derived using different calibration methods will have different dependencies on photon energy (see section 6.4.4, Figure 26). A presentation of the energy dependence should therefore always include a specification of the particular choice of P_{KA} that has been used.

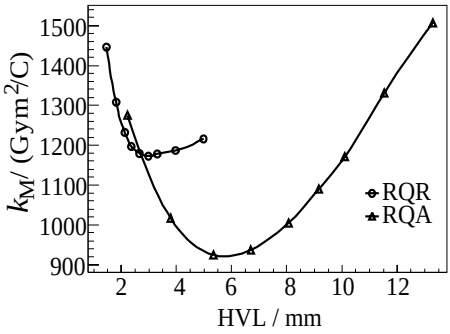

Figure 13. Calibration coefficients for a Master KAP-meter (KM1) as a function of HVL in mm of Al for two different sets of reference radiation qualities RQR and RQA (ISO 4037, IEC 61267). The data were obtained from PTB (Figure 4 in Paper V) for radiation incident on the KAP-meter.

Using calibration method 2 according to the procedures described in Paper I, it is both tedious and difficult to determine the energy dependence experimentally for a broad range of tube voltages and beam filtrations. Another quantity, the sensitivity, *S*, that can easily be measured, was used instead to study the energy dependence experimentally. The sensitivity describes the energy dependence of k_1 and its ability to describe the energy dependence of k_2 and k_3 is discussed in section 6.1. Monte Carlo simulations were used to analyze the experimental results and to assess the contributions from the different influencing factors (see equation (5)) in a way impossible to achieve with measurements. However, measured data are important and give the net results from all the influencing factors, including those that were difficult (or required a lot of extra work) to include in the Monte Carlo model such as the heel effect and extra-focal radiation. In addition, the geometry of the KAP-meter was somewhat simplified in the Monte Carlo simulations. This was, however, not believed to have a major effect on the results.

The energy dependence of the KAP-meter calibration coefficients is not easily described. Overviews of the Monte Carlo simulations and measurements of sensitivity that have been performed in Paper IV and Paper V and the quantities derived from these data are shown in Figure 14 (a) Monte Carlo simulations and (b) measurements.

In the following subsections, the concept of sensitivity is defined. A short description of the materials and methods used in the Monte Carlo simulations and in the measurements is given and this is followed by presentations and discussion of results.

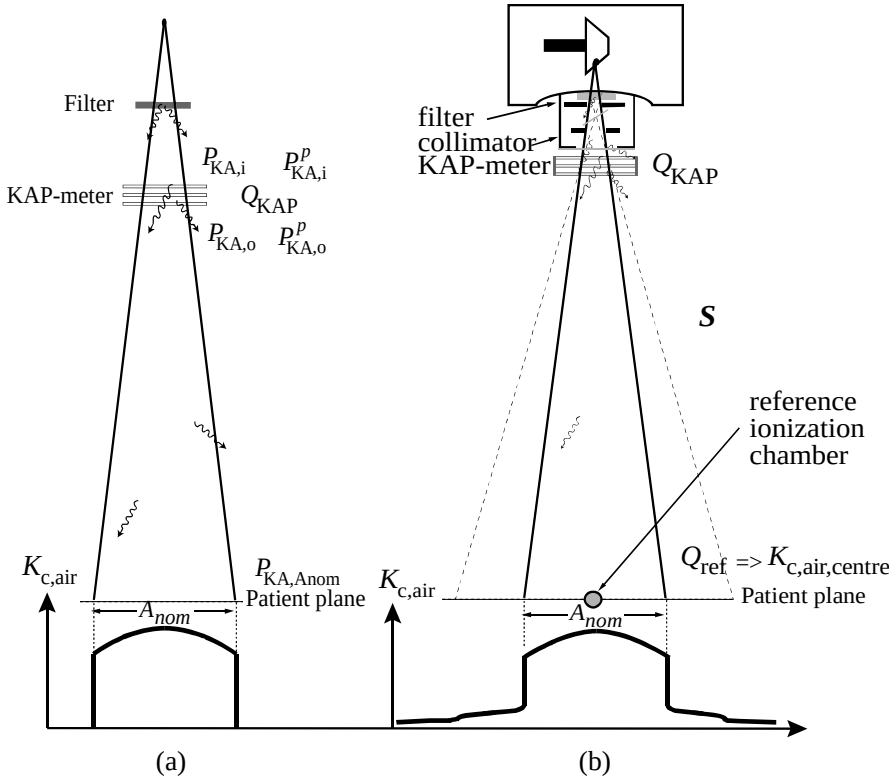

Figure 14. (a) The geometry of the Monte Carlo simulations and quantities derived using these simulations. (b) The measurement geometry and quantities derived.

6.1. The sensitivity (*S*) and the field homogeneity factor (*F*)

The calibration coefficient *k* (equation (2)) may be written in a simplified way as

$$k = \frac{P_{KA,r}}{Q_{KAP}} = \frac{P_{KA,r}}{K_{c,air,centre} A_{nom}} \frac{K_{c,air,centre}}{Q_{KAP}} A_{nom} = FS^{-1} A_{nom}, \qquad (14)$$

where $K_{c,air,centre}$ is the air collision kerma measured at the crossing of the reference plane and the beam axis and A_{nom} the nominal beam area at the reference plane. The KAP-meter sensitivity, *S*, and the field homogeneity factor, *F*, are defined as

$$S = \frac{Q_{\mathrm{KAP}}}{K_{\mathrm{c,air,centre}}}, \tag{15}$$

$$F = \frac{P_{\mathrm{KA,r}}}{\mathrm{K}_{\mathrm{c,air,centre}} A_{\mathrm{nom}}}. \tag{16}$$

The sensitivity, S, is a useful quantity since it is calculated from Q_{KAP} and $K_{\mathrm{c,air,centre}}$, quantities that are easily measured with a KAP-meter and an ionization chamber. The sensitivity S depends on the beam aperture (and position of additional filters, see section 6.5.) and therefore, when used to compare the energy dependences of different KAP-meters, the experimental geometry must be the same. In general, the field homogeneity factor, F, is not a constant but its dependence on photon energy is expected to be considerably lower than the that of the sensitivity, S, as long as the irradiation geometry is not changed. It is further noted that the energy dependence of the calibration coefficients derived according to method 1 ($k_1 = \frac{K_{\mathrm{c,air,centre}} A_{\mathrm{nom}}}{Q_{\mathrm{KAP}}}$) is closely related to that of S^{-1} since A_{nom} (= A_{film} or $A_{\mathrm{sq.law}}$) is constant and not expected to vary with photon energy.

6.2. Monte Carlo simulations

6.2.1. Monte Carlo codes.

Simulations were performed using the MCNP5 (X-5 Monte Carlo Team 2004) Monte Carlo code (Paper IV) and the pencyl code from the PENELOPE 2003 package (Baró *et al* 1995) to calculate the sensitivity, S, in Paper V.

6.2.2. Simulations using MCNP

The MCNP5 code was used in Paper IV to calculate values of $P_{\mathrm{KA,Anom}}$, $P_{\mathrm{KA,o}}$, $P_{\mathrm{KA,i}}$, and $P_{\mathrm{KA,i}}^{\mathrm{p}}$ from equation (5). Values of k and S were also calculated from equations (2) and (15) respectively.

The MCNP5 simulation geometry consisted of a point source, a KAP-meter, and an optional additional filter, see Figure 15. Three configurations were studied:

(A) The additional filtered was not used
(B) The additional filter was placed closely in front of the KAP-meter
(C) The additional filter was treated analytically as an ideal non-scattering filter (corresponding to a position upstream of the collimator close to the focus).

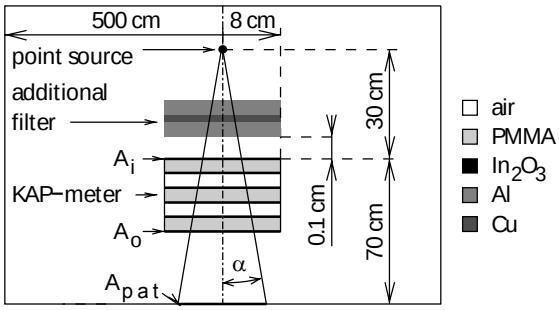

Figure 15. Schematic view of the geometry used in the Monte Carlo simulations. The KAP-meter and the additional filter were represented by a set of cylinders with radius 8 cm enclosed in a cylinder with radius 5 m and height 1 m. The entrance, exit, and patient planes are denoted by A_i, A_o, and A_{pat}, respectively. In cases A and C, simulations were performed with the filter removed. The sensitive area, A_s, of the KAP-meter equals A_o with radius 8 cm (Figure 3 in Paper IV).

The point source emitted photons into a cylindrical cone with apertures α= 3º, 6º, 9º, and 12º corresponding to circular beam areas with diameter 10, 21, 32, and 42 cm respectively at 1 m distance from the source. X-ray spectra corresponding to tube voltages 40, 50, . . ., 140 kV were taken from the catalogue of diagnostic x-ray spectra (Cranley *et al* 1997). They were analytically filtered with 5 mm Al to account for the attenuation in the x-ray tube window and close-to-focus filters. In case C, an additional analytical filtration of 2 mm Al and 0.15 mm Cu was applied. In case B, this additional filter was part of the geometry.

The KAP-meter consisted of three cylindrical PMMA walls coated with indium oxide (In_2O_3) and two cylindrical air cavities, all with the radius of 8 cm. The thicknesses of the outer and inner walls were 1.5 mm and 1.0 mm respectively and those of the air cavities was 5.7 mm. Material composition and thickness resembled that of KM3, the thickness of the conducting layers of indium oxide being supplied by the manufacturer on condition of our keeping them confidential. To speed up calculations, the rectangular electrodes of KM3 were replaced by cylinders. The source - KAP-meter distance was 30 cm and the source - patient plane distance 1 m. Transport of photons and electrons was simulated using the detailed physics treatment of MCNP5. Results were normalized per unit photon emitted into the solid angle 4π from a point isotropic source.

The integration regions A_i and A_o were equal to the entrance and exit surfaces, respectively, of the cylindrical KAP-meter. Integration region A_{pat} was equal to the primary beam area at the patient plane (which complies with $A_{sq.law}$ and A_{film} in equation (7) and equation (8)).

6.2.3. Simulations with the Pencyl code from PENELOPE

To calculate the values of the sensitivity, *S*, the pencyl code from PENELOPE and equation (15) were used. PENELOPE was selected because of its more detailed physics (than MCNP5) in simulating interaction processes in the thin conducting layers and the energy imparted to the KAP-meter air layers. A geometry similar to that in Figure 15 was used in the simulations. The point source emitted monoenergetic photons into a circular cone with the aperture α=7.24º, chosen to coincide with the aperture used in the measurements of the sensitivity. The KAP-meter was approximated as a series of cylinders of radius 80 mm. The computation was run in the detailed mode in which PENELOPE performs collision by collision simulation. Calculations were performed for a set of photon energies ranging from 5 to 150 keV. In order to display the effects of the various physical parameters influencing the sensitivity, simulations were performed in the same geometry using different wall materials (PMMA, Trogamid, dense air), and coating materials of graphite and In_2O_3 of varying thicknesses including zero thickness. $K_{c,air,centre}$ was calculated analytically disregarding contributions from scattered radiation (found to contribute less than 1% to the total $K_{c,air}$ on the beam central axis in Paper IV).

The collected charge, Q_{KAP}, was assumed to be proportional to the energy imparted (ε) to the air layers in the KAP-meter. To study the effect of the K- and L- absorption edges, simulations of ε were performed with monoenergetic photons and the resulting values were then integrated over analytically filtered x-ray spectra (1 mm Al, 5 mm Al, and 5 mm Al + 0.15 mm Cu). Anode angle 15º and constant potential were used, see Paper V for details.

6.3. Measurements of sensitivity, *S*

6.3.1. Equipment used in the measurements

Three types of KAP-meter were used: KM1, KM2 (previously described in section 5.2.1), and KM3 (type 70157, VacuTec Gmbh, sold in Sweden by RTI electronics as Doseguard 100), see Table 2 and Figure 16. Thicknesses of conducting layers of KM1 and KM3 were supplied by the manufacturers on condition of our keeping them confidential. The thickness of the conducting graphite layer in KM2 was estimated using a DEKTAK profile meter (mod. 3030).

$K_{c,air,centre}$ was measured with a spherical reference ionization chamber (Shonka-Wyckoff model A3) with calibration coefficients traceable to BIPM. The energy dependence of this chamber was found to be small and the uncertainties in the $K_{c,air,centre}$ measurements were estimated to be ± 1.3% (coverage factor 2, Type B estimation), see Paper V for more details. Irradiation was performed using a Siemens x-ray tube (Bi 150/30/50R) with anode angle 15º and a constant potential generator (OY Medira AB).

Table 2 Construction details of KAP-meters. Thicknesses of Trogamid T ($C_{17}H_{24}N_2O_2$) and PMMA ($C_5H_8O_2$) walls are given for the upper, middle, and lower electrodes. The thickness of the In_2O_3:Sn coating is confidential (from Paper V).

	wall		coating		cavity	
label	material	thickness (mm)	material	thickness (μm)	material	thickness (mm)
KM1	Trogamid T	1.85, 1.02, 1.85	In_2O_3:Sn	confid.	air	6.34
KM2	PMMA	2.0, 2.0, 2.0	carbon	10	air	4.0
KM3	PMMA	1.5, 1.0, 1.5	In_2O_3:Sn	confid.	air	5.9

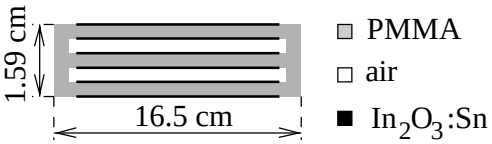

Figure 16. Schematic side view of the KM3. The quadratic surface area of the KAP-meter is 165 mm x 165 mm. The size and construction of KM1 and KM3 are similar, see the text for details (from Paper V).

The charge from the KAP-meter, Q_{KAP}, and the air kerma, $K_{c,air,centre}$, at the reference position, see Figure 17, were measured simultaneously. The sensitivity S was calculated from equation (15). Measurements were performed at tube voltages in the range 40 - 140 kV and total filtrations of 1 mm Al, 5 mm Al, and 5 mm Al +0.15 mm Cu. The large distance (80 cm) between the reference chamber and the KAP-meter was selected to decrease the possible influence from radiation scattered from the KAP-meter walls and because it represents a typical patient geometry. The extra collimator of lead, 5 mm thick, with a circular aperture of diameter 30 mm was positioned 11.8 cm from the focal spot and defined a circular beam of diameter 76.3 mm at the position of the KAP-meter.

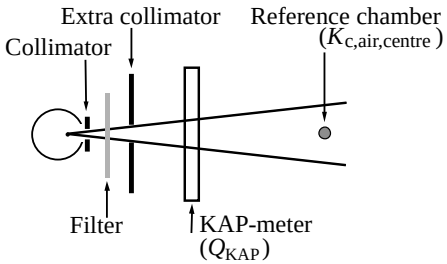

Figure 17. Experimental set-up for measuring the sensitivity (see text for explanation). The housing for the adjustable collimators was replaced with a single lead collimator (5 mm thick) with a circular aperture with diameter 30 mm. The filter, collimator, KAP-meter and reference chamber were placed 6, 11.8, 30 and 110 cm respectively from the focal spot.

6.3.2. Added filter on top of the KAP-meter

The effects of scatter from a test filter (1 mm Al+0.15 mm Cu+1 mm Al) were investigated using the experimental set-up shown in Figure 17. The ordinary collimator near the focus was used, the extra collimator was removed and the KAP-meter (KM1) was placed at 40 cm from the focal spot. Two total filtrations were used, 0.5 and 3 mm Al (excluding the test filter), respectively. The test filter was positioned at different distances from the KAP-meter. Readings from the KAP-meter, Q_{KAP}, and reference chamber, $K_{c,air,centre}$, were recorded at tube voltages 40, 90 and 140 kV. All readings were normalized with the filter positioned 29 cm from the KAP-meter. The field was circular with diameter 9 cm at the entrance plane of the KAP-meter. The reference chamber was placed 110 cm from the focal spot.

6.4. Results and discussion

The aim of this subsection is to analyze the factors influencing the energy dependence of calibration coefficients. This is not a straightforward task since the interaction between different influencing factors may be non-negligible.

6.4.1. Effects of KAP-meter wall material, and atomic composition and thickness of conducting layers

Figure 18 shows values of the sensitivity, *S*, calculated from Monte Carlo simulations for a number of fictitious KAP-meters. As a starting point a KAP-meter with air-equivalent walls was simulated (the geometrical configuration of KM3 was assumed with the PMMA layers replaced by equally thick layers of air of density 1.19 g/cm^3). The sensitivity for the fictitious KAP-meter in case a) (Figure 18) decreases slowly with increasing tube voltage due to the attenuation in the middle and exit walls (attenuation in the entrance wall decreases the signals of both the KAP-meter and the reference chamber). In addition, scatter from the three KAP-meter walls influences the dependence on tube voltage and filtration. In case b), a 10 μm carbon coating is added to the air equivalent walls resulting in a decrease in sensitivity of 15-30% depending on tube voltage and filtration. The thickness of the carbon coating is not sufficient to provide electronic equilibrium of the electrons from the carbon in the air cavities of the KAP-meter but is large enough to lower substantially the numbers of secondary electrons in the air cavities due to the lower atomic number of carbon compared to the effective atomic number of air. The importance of the secondary electrons is further demonstrated, although in the opposite sense, when coating of indium oxide is used. The sensitivity increased approximately 2 times and 15 times when adding indium oxide coating of thickness identical to that of KM3 (confidential) and of 300 nm, respectively (case c and d*). The reason is the substantially increased probability of the photoelectric effect due to the high atomic number of indium (Z=49). Simulations with different thickness of the indium oxide layer showed that the increase in sensitivity was

almost linear with the thickness of the coating. The energy dependence, however, also increases with increasing thickness of the indium layer, in particular, for the lower tube voltages.

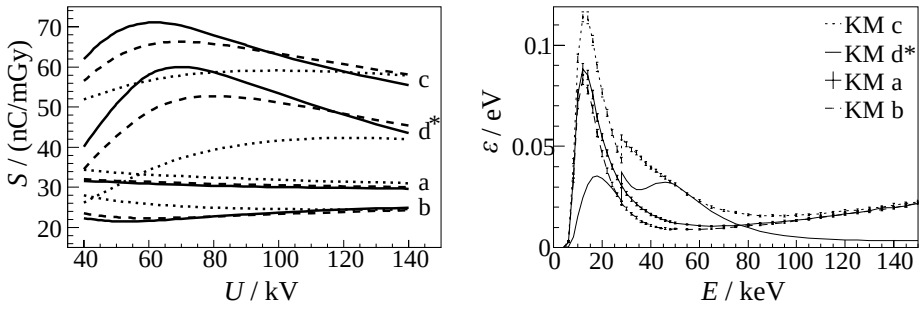

Figure 18. Left: The sensitivity, *S*, as a function of tube voltage, *U*, calculated from Monte Carlo simulations for a set of fictitious KAP-meters a) air-equivalent walls and coating; b) air-equivalent walls, 10 μm carbon coating; c) air-equivalent walls coated with indium oxide of the same thickness as KM3; d) air-equivalent walls coated with indium oxide with thickness 300 nm. The * indicates that values of *S* corresponding to case d are divided by 10. The air-equivalent walls have a density of 1.19 g/cm^3 (same as KM3). For each KAP-meter, curves corresponding to total filtrations of 1 mm Al (….), 5 mm Al (- - -), and 5 mm Al + 0.15 mm Cu (___) are drawn. The component of uncertainty arising from random effects are less than 1% (3σ). Right: Simulated energy imparted, ε, to the air cavity as a function of photon energy, *E*, for KAP-meter a) (___), b) (- - -), c) (….), and d*) (___). The order of the curves at a photon energy of 40 keV corresponds to the order of the notations in the upper right corner of the diagram. Values of ε corresponding to case d are divided by 10 and error bars are omitted. The isotropic point source emits 1 photon into the solid angle 4π. Error bars show the component of uncertainty arising from random effects (±3σ) (from Paper V).

For all simulated cases the coating is too thin to prevent electrons liberated in the walls from reaching the air cavities and thus the electrons (photo-, Auger-, and Compton electrons) contributing to the energy imparted to the air volume are a mixture of electrons originating from the wall, the coating and air. The relative contributions from different layers are strongly dependent on photon energy and the atomic number and thickness of the coating layers. The influence of electrons generated in In_2O_3 is most clearly demonstrated in the simulation of the thickest (300 nm) In_2O_3 layer (case d*). Photons with energies lower than about 5 keV are mostly absorbed in the KAP-meter front wall. Above 5 keV, the energy imparted to the air volume increases strongly with increasing photon energy due to an increasing fraction of the incident photons and to an increasing number of L-shell photoelectrons from indium that reach the air volume. The decrease with increasing photon energy between 18 and 28 keV is due to a decreasing probability for the photoelectric effect in the L-shell. The edge at 28 keV corresponds to the K-edge of indium and subsequent emission of Auger electrons. The photoelectrons are not energetic enough to reach the air volume, and even if they do, they have very little energy to impart to it. The decrease with

increasing energy above 28 keV depends on the decreasing probability for photoelectric interaction with K-shell electrons. At about 35 keV the curve increases again due to the increasing energy of the K-shell photoelectrons which can reach the air volume from increasing depths in the coating and have increasing energy to impart to it. Above about 45 keV, the effect of the decreasing probability of the photoelectric effect results in decreasing energy imparted to the air volume with increasing energy. At higher energies, Compton electrons from both the indium oxide layer and PMMA contribute the major part of the energy imparted to the air volume. The decreasing interaction coefficient combined with increasing energy of the liberated Compton electrons results in an approximately constant value of ε.

To quantify the influence from the non-air equivalence of the coating material the formalism used in Paper V, equation (4), may be used to express the sensitivities, S_a, S_b, S_c and S_{d*} corresponding to the different fictitious KAP-meters a, b, c and d*, respectively, in Figure 18. For example, the quotient S_c/S_a can be expressed as

$$\frac{S_c}{S_a} = \frac{Q_{KAP}(In_2O_3)}{Q_{KAP}(air)} = \frac{\left[(\overline{D}_{air})m_{air}\frac{e}{W}\right]_{In_2O_3}}{\left[(\overline{D}_{air})m_{air}\frac{e}{W}\right]_{air}} = \frac{(\overline{D}_{air})_{In_2O_3}}{(\overline{K}_{c,air})_{air}}, \qquad (17)$$

where $(\overline{D}_{air})_{In_2O_3}$ is the absorbed dose in air averaged over the active air volume for the indium coated KAP-meter. $(\overline{K}_{c,air})_{air}$ is the air collision kerma averaged over the active air volume for the air-coated KAP-meter and m_{air} the mass of the air layers (the same in both KAP-meters). Due to the conditions of charge particle equilibrium in the air-coated KAP-meter (case a), the absorbed dose to air equals the air-collision kerma in this chamber. The ratio in equation (17) quantifies the effects of the lack of charged particle equilibrium in the air volume of KAP-meter c (In_2O_3 coating of the same thickness as KM3) and is shown in Figure 19 as a function of photon energy. Corresponding ratios for two other KAP-meters with coatings 10 μm carbon (b) and 300 nm In_2O_3 coating (d*) are also shown in Figure 19. In all three cases, the coatings are thin and the influence on the energy fluence in the air cavity due to attenuation and scattering in the coatings is expected to be negligible. Characteristic K- and L-shell radiations from the indium oxide layer may possibly contribute to the ratio in equation (17) increasing $(\overline{D}_{air})_{In_2O_3}$ in the nominator.

The quotients of $(\overline{D}_{air})_{In_2O_3}$ to $(\overline{K}_{c,air})_{air}$ in the air cavities for the indium oxide coated KAP-meters have a peak at photon energies between 28 and 70 keV (note that the values of energy imparted for the 300 nm case, d*, are divided by 10). This explains the difference in

the dependence of the sensitivity on tube voltage at different filtrations in Figure 18. At a total filtration of 1 mm Al, the x-ray spectra are broad and the effect on the sensitivity of an increased tube voltage is smeared out. At total filtrations of 5 mm Al and 5 mm Al +0.15 mm Cu, the spectra are much narrower and, due to substantially higher fractions of photons in the energy range 28-70 keV at these tube voltages, pronounced peaks are obtained at about 60-70 kV. In the case of a total filtration of 1 mm Al, increasing the tube voltage above 70 kV gives an increase in the relative fraction of photons in the range 28-70 keV and the sensitivity curve in Figure 18 continues to increase.

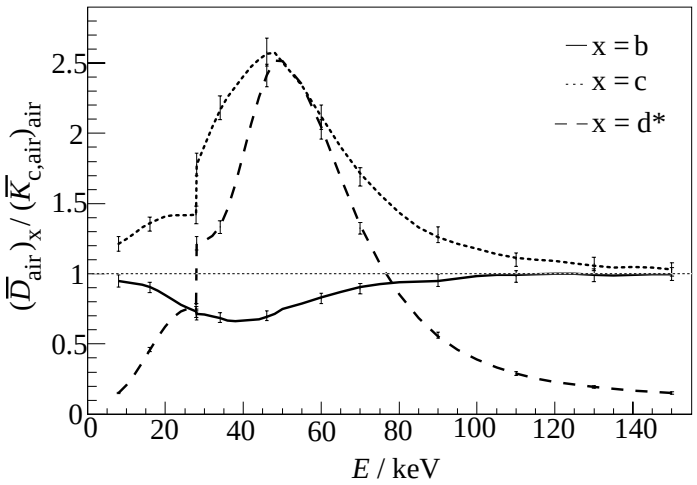

Figure 19. Quotients of $(\overline{D}_{air})_x$ to $(\overline{K}_{c,air})_{air}$ in the KAP-meter air cavities for different coatings *x* calculated by Monte Carlo simulations. Case b: 10 μm carbon coating. Case c: indium oxide coating with thickness the same as in KM3. Case d*: 300 nm indium oxide coating (values divided by 10). The error bars show the component of uncertainty arising from random effects (3σ).

Figure 20 shows Monte Carlo simulated sensitivities of the meters KM1, KM2 and KM3. The influence from the non-air equivalence of the KAP-meter walls can be evaluated by comparing curve c in Figure 18 (dense air walls and In_2O_3 coating of the same thickness as KM3) with the curve for KM3 in Figure 20 (PMMA walls and In_2O_3 coating of the same thickness as KM3). The ratio S_{PMMA}/S_{air} can be expressed as

$$\frac{S_{PMMA}}{S_{air}} = \frac{\left[\frac{\overline{D}_{air} m_{air}}{K_{c,air,centre}} \frac{e}{W}\right]_{PMMA}}{\left[\frac{\overline{D}_{air} m_{air}}{K_{c,air,centre}} \frac{e}{W}\right]_{air}} = \frac{(\overline{D}_{air})_{PMMA}}{(\overline{D}_{air})_{air}} \frac{(K_{c,air,centre})_{air}}{(K_{c,air,centre})_{PMMA}}, \qquad (18)$$

where the indexes PMMA and air indicate the KAP-meter wall material (with the same thickness of In_2O_3 coating).

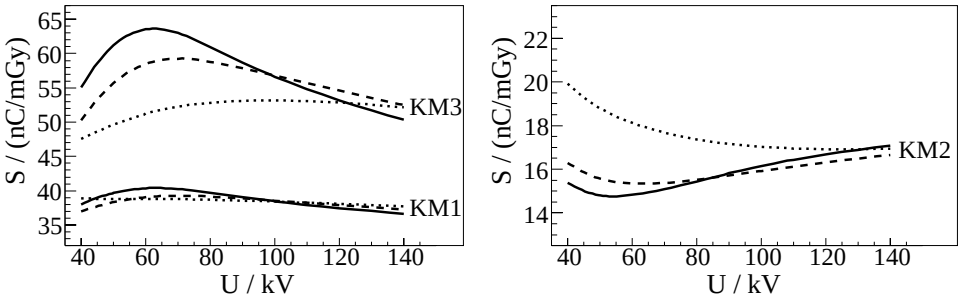

Figure 20. The sensitivity, *S*, as a function of tube voltage, *U*, calculated from Monte Carlo simulations for KM1, KM2, and KM3. For each KAP-meter, curves for total filtrations of 1 mm Al (…..), 5 mm Al (- - -), and 5 mm Al + 0.15 mm Cu (___) are drawn. The isotropic point source emits 1 photon into the solid angle 4π. The component of uncertainty arising from random effects is less than 1% (3σ).

The sensitivity for the KAP-meter with PMMA walls (and In_2O_3 coating) is decreased by about 10% as compared to air walls (and In_2O_3 coating), see Figure 21 (a). The corresponding ratio as a function of photon energy is shown in Figure 21 (b).

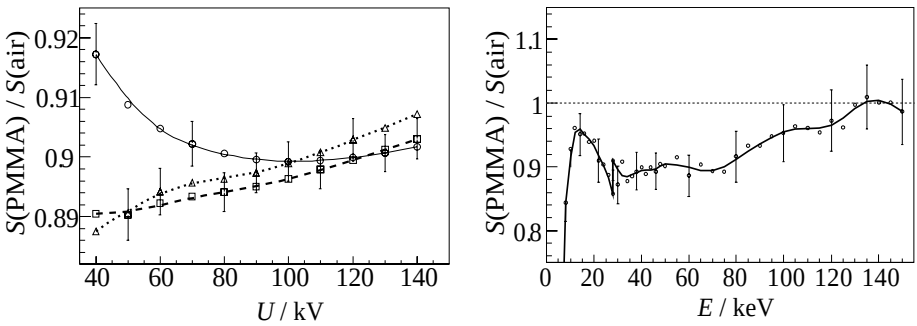

Figure 21. (a) Ratio *S*(PMMA-walls)/*S*(dense-air-walls) for KAP-meters with the same thickness of In_2O_3 coating, see equation (18), calculated from Monte Carlo data as a function of tube potential, *U*, for three different total filtrations; 1 mm Al (○), 5 mm Al (□), and 5 mm Al + 0.15 mm Cu (△). The KM3 geometry and coating were used in the simulations. (b) The same ratio as a function of photon energy. The error bars show the component of uncertainty arising from random effects (3σ).

The dependence of the quotient $S_{\text{PMMA walls}}/S_{\text{air walls}}$ (with In_2O_3 coating) on tube voltage is small. The quotient decreases by about 1.5% for tube voltages between 40 and 140 kV for the 1 mm Al filtration and increases by about 1.5% for the same tube voltage interval and filtrations of 5 mm Al and 5 mm Al + 0.15 mm Cu. Thus the energy dependence of the

sensitivity due to the non-air equivalence of the KAP-meter walls is of minor importance for the overall energy dependence.

6.4.2. Influence from choice of reference plane and area of integration

The values of different factors in equation (5) were calculated by Monte Carlo simulations and show how P_{KA} varies when different reference planes and areas of integration are used. Values of the ratios $P_{KA,Anom}/P_{KA,o}$, $P_{KA,o}/P_{KA,i}$, $P_{KA,i}\big/P^{p}_{KA,i}$, and $P^{p}_{KA,i}\big/(A_s\overline{D}_{air})$ are shown in Figure 22.

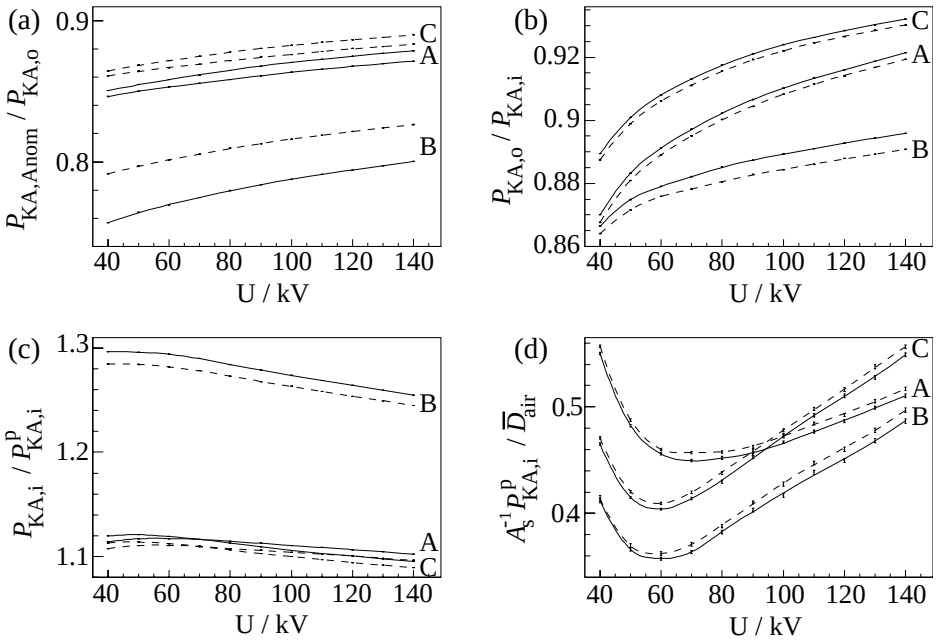

Figure 22. Ratios $P_{KA,Anom}/P_{KA,o}$ (a), $P_{KA,o}/P_{KA,i}$ (b), $P_{KA,i}\big/P^{p}_{KA,i}$ (c), and $P^{p}_{KA,i}\big/(A_s\overline{D}_{air})$ (d) as functions of tube voltage U for cases A, B, and C and beam apertures 3º (—) and 12º (--). In case A, the additional filter was not used; in case B, the additional filter was placed closely in front of the KAP-meter, and case C, the additional filter was treated analytically as an ideal non-scattering filter (from Paper IV).

The ratio $P_{KA,Anom}/P_{KA,o}$ (Figure 22 (a)) essentially shows the amount of photons scattered in the KAP-meter, air, and filter that pass outside A_{nom} in the patient plane while still contributing to $P_{KA,o}$. Compared to $P_{KA,o}$, the relative decrease in $P_{KA,Anom}$ was about 11-16% for cases A and C and 18-24% for case B. The absolute value of the quotient is,

especially in case B, dependent on the beam area, while the variation with the tube voltage is almost the same for the different beam areas. The difference between case A and case C probably arises because at higher energies more of the photons are scattered in the forward direction (and thus a larger fraction of the photons will pass inside A_{nom} in the patient plane). The same is true in case B, but here, in addition to the air and the KAP-meter, the filter acts as an additional source of scattered photons resulting in considerably lower values of $P_{KA,Anom}/P_{KA,o}$ than in cases A and C.

The ratio $P_{KA,o}/P_{KA,i}$ (Figure 22 (b)) shows the relation between P_{KA} at the exit side of the KAP-meter and at the entrance side. Due to the attenuation in the KAP-meter wall and differences in the contributions from scattered photons in the KAP-meter, $P_{KA,o}$ was about 7-14% smaller than $P_{KA,i}$. The dependence on beam area was small, less than 0.5% in cases A and C and only slightly higher in case B. The decrease in the quotient at larger beam areas is due to an increased fraction of photons impinging on A_i but not on A_o as the distance between the beam edges and the boundaries of the KAP-meter decreases.

The ratio $P_{KA,i}\big/P^{p}_{KA,i}$ (Figure 22 (c)) quantifies the backscatter from the KAP-meter that is about 10% for cases A and C and about 26% for case B. The variation with tube voltage is about 2% in cases A and C, slightly larger in case B, about 3%.

The ratio $P^{p}_{KA,i}\big/(A_s\overline{D}_{air})$ (Figure 22 (d)) describes the combined effect of scatter and attenuation in the KAP-meter walls and the non-air equivalence of the conductive coatings. This effect dominates the energy dependence of all of three calibration coefficients (k_1, k_2 and k_3) and the variation is more than 30%. Case A has a different dependence on the tube voltage than cases B and C due to the lower total filtration, 5 mm Al in case A as compared to 7 mm Al + 0.15 mm Cu in cases B and C. The curves corresponding to cases B and C are almost parallel indicating that scattered photons have a small influence on the variation of the quotient with tube voltage.

The ratio $P^{p}_{KA,o}\big/P^{p}_{KA,i}$ shows the effect of the attenuation in the KAP-meter walls on P_{KA}, see Figure 23 (a). The ratio is (within 0.2%) independent of beam aperture indicating that, due to the oblique incidence, the increased attenuation of the photons in the outer parts of a large aperture (12°) beam is negligible as compared to a small beam. The influence of scatter from the KAP-meter walls can be evaluated by the ratio $P_{KA,o}\big/P^{p}_{KA,o}$ shown in Figure 23 (b). With an aperture of 6° the scatter in the KAP-meter increases the values of $P_{KA,o}$ by about 14% at 40 kV and about 12.5% at 140 kV as compared to $P^{p}_{KA,o}$.Thus, at high tube voltages, the increase in $P_{KA,o}$ due to photons scattered from the KAP-meter walls, is higher than the decrease duo to the attenuation in the walls.

The scatter contribution shown in Figure 23 (b) agrees well with the figures in Figure 22 (a) indicating that the major part of the contribution to $P_{KA,o}$ from photons scattered in the KAP-meter will not contribute to the $P_{KA,Anom}$ in the patient plane.

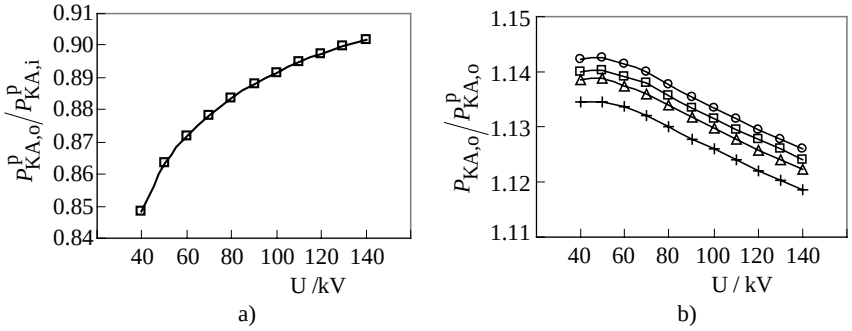

Figure 23. a) Shows ratio $P^p_{KA,o}/P^p_{KA,i}$ for beam aperture 6º (□). b) Shows ratio $P_{KA,o}/P^p_{KA,o}$ for beam apertures 3º (○), 6º (□), 9º (△), and 12º (+). Both ratios are shown as a function of tube voltage, *U*, at a total filtration of 5 mm Al (case A). $P^p_{KA,o}$ and $P^p_{KA,i}$ are the contributions to P_{KA} from primary photons at the exit and entrance surfaces of the KAP-meter respectively.

Figure 24 shows measured values of the sensitivity *S* for meters KM1 and KM3 (left) and KM2 (right). Let Δ be a quantity describing the variation of the sensitivity with tube voltage for a specific total filtration defined as: $\Delta=(S_{max}- S_{min})/S_{max}$. KM1 and KM3 are both In_2O_3-coated with similar values of Δ of about 10%, 14% and 17% at total filtrations of 1 mm Al, 5 mm Al and 5 mm Al+0.15mm Cu, respectively. The graphite-coated KAP-meter (KM2) has a sensitivity a factor of 3 lower compared to both KM1 and KM3, a different shape of energy dependence curve and lower Δ-values as compared to KM1 and KM3 (8%, 4% and 9% at total filtrations of 1 mm Al, 5 mm Al and 5 mm Al+0.15mm Cu respectively).

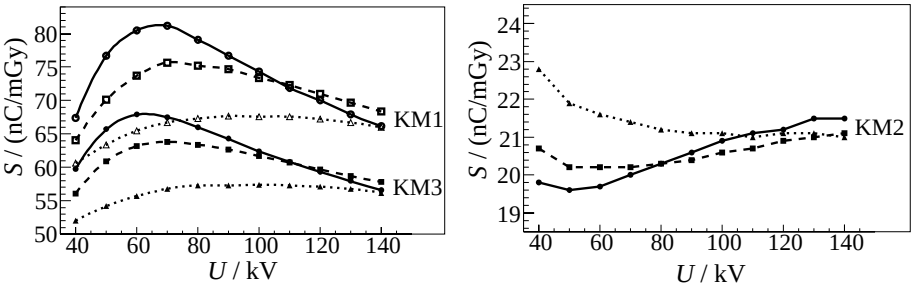

Figure 24. Left: Measured values of sensitivity, *S*, as a function of tube voltage, *U*, for KM1 and KM3. Right: the corresponding curves for KM2. For each KAP-meter, curves corresponding to total filtrations of 1 mm Al (…) , 5 mm Al (- - -), and 5 mm Al + 0.15 mm Cu (___) are drawn.

6.4.3. Comparison between experimental results and Monte Carlo simulations

The Monte Carlo simulations were performed in order to demonstrate the physical factors underlying the energy dependence of the calibration coefficient. It was thus not the aim here to verify the Monte Carlo simulations in which case more efforts should have been made to assure that the irradiation geometry and beam qualities were the same, i.e., the square form and side walls of the KAP- meter should have been simulated and identical energy spectra been used (tube voltage and HVL). Still it is interesting to compare the experimental and simulated values of the sensitivities. The difference D ($D = (S_{Measured}-S_{MonteCarlo})/ S_{Measured}$) is shown in Figure 25 as a function of tube voltage with beam filtration as parameter. For the KM1 there is a difference in sensitivity values of about 40-50% as compared to the Monte Carlo simulated data. Better agreement is obtained for the KM3 (less than 10% difference). The major part of the discrepancy for the KM1 is believed to depend on a discrepancy between the real thickness of the indium oxide layer and the one used in the Monte Carlo calculations as given by PTW and valid for KAP-meters manufactured 2004. KM1 used in the experiments is 15 years old and the results indicate a thicker conducting layer than for KAP-meters manufactured today. Possibly the manufacturer has decreased the thickness on modern KAP-meters in order to decrease its energy dependence. Discrepancies may also be due to differences between the energy spectra used in the experiments and in the simulations. To assure that the energy spectra were identical, the HVLs for the spectra used in the measurements were compared to the HVLs calculated from the corresponding spectra used in the simulations as obtained from the catalogue of diagnostic x-ray spectra (Cranley *et al* 1997). Although several attempts were made to mimic the HVL's from the measurements by adding extra Al filter to the spectra from the catalogue, it was not possible to get a perfect fit to the HVLs for the whole range of tube voltages and added filters used (40-140 kV). On the other hand, eventual differences in the simulated spectra may be of minor importance compared to the energy dependence of the KAP-meter sensitivity caused by the thickness of the indium oxide layer, see Figure 19. It is here interesting to note that the discrepancy between the experimental and calculated sensitivities for the KM3 is essentially independent of the beam quality whereas that of KM1 clearly depends on beam quality. This could be interpreted as being due to the discrepancy between the thickness of the indium oxide layer used in the experiments and calculations for the KM1while the correct thickness was simulated for KM3. In the case of KM2, the beam quality depending discrepancy may be influenced by the presence of an unknown binding material in the graphite coating. The discrepancy between the experimental and simulated results may also be caused by the neglect of the heel effect and extra-focal radiation in the simulations. Other shortcomings of the Monte Carlo code such as inaccurate interaction cross sections and difficulties to simulate interface effects when thin layers of a material are handled, so that

multiple scattering theories are no more valid, may also exist. Effects of disregarding the heel effect and extra-focal radiation are discussed below.

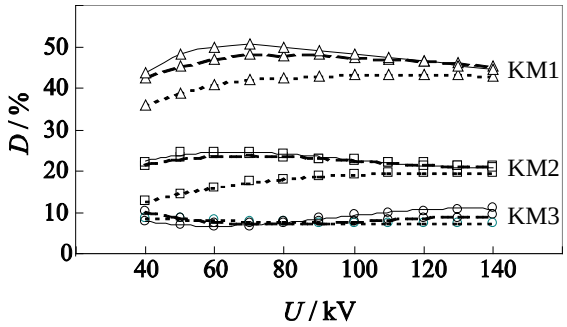

Figure 25. Differences between measured and Monte Carlo calculated values of sensitivity for KM1, KM2 and KM3. The difference D is calculated as $(S_{Measured}-S_{MonteCarlo})/ S_{Measured}$ for each KAP-meter. Curves corresponding to total filtrations of 1mm Al (….), 5 mm Al (---) and 5 mm Al + 0.15 mm Cu (___) are shown.

Two consequences of the heel effect are that (1) the energy spectrum and (2) the $K_{c,air}$ vary with position in the beam. In order to examine the influence of the variation of the energy spectrum on the sensitivity, spectra for three different anode angles were used to simulate the energy spectra at about 9 cm (at 100 cm from the focal spot) from the central axis in the anode direction, 9 cm in the cathode direction and at the central axis. The differences in the first and second spectra, as compared to that on the central axis, were found mainly in the low-energy region, below 30 keV. The sensitivity calculated using those spectra was then compared to the sensitivity using the central axis spectra. Only small differences were found except for the spectra with 1 mm Al filtration where the maximum deviation in sensitivity was found at a tube voltage of 70 kV being about 5% and 2.7% for the graphite and indium oxide coated KAP-meter, respectively. In a real x-ray field, the energy is gradually changing over the field area and the corresponding change in sensitivity is less pronounced. The second effect of the heel effect is that the $K_{c,air}$ varies in the cathode anode direction. The $K_{c,air}$ on the central axis is higher than $K_{c,air}$ averaged over the whole beam area to a degree increasing with increasing field area. For the actual geometry and energy spectra used the deviation between $K_{c,air,centre}$ and $K_{c,air}$ averaged over the beam area was estimated using data from Ay *et. al.* to be less than 2-4%. Omission of the heel effect in the simulations will thus result in sensitivities that are 2-4 % too high. Correcting for this, however, contributes to increase the difference between experiments and simulations. The influence from extra-focal radiation is more difficult to evaluate. It contributes to a deviation of $K_{c,air,centre}$ from the inverse square law, resulting in a steeper decrease of $K_{c,air,centre}$ along the central axis. The effect is larger the smaller the beam aperture. From Figure 10 the deviation from the inverse square law was estimated to be between 3% and 9% at 100 cm focal distance for

beam apertures between 9.8° and 2.2°. Thus, the Monte Carlo simulations may underestimate the measured sensitivity with about 5% counteracting the overestimate due to the heel effect. The fact that the extra focal radiation has lower energies (Larsson *et.al.*1996) and different angles of incidence on the KAP-meter is not assumed to have any major effect on the simulated values of Q_{KAP}. Finally, the indium oxide is doped with tin to a degree that may amount to as much as 10%. Neglecting the effect of the doping material, the simulated values of Q_{KAP} may be underestimated by 1-2%.

6.4.4. Variation of the calibration coefficients

Study of the energy dependence of the sensitivity is a substitute for studying that of the calibration coefficients. However the calibration coefficient k_1 is expected to vary as S^{-1} while k_3 is not. As pointed out in section 5.5 the value of k_1 depends on the particular x-ray installation and the calibration geometry while the value of k_3 is independent of the geometry and can be applied at any x-ray installation. The difference between those two calibration coefficients can be evaluated by calculating the quotient (see equations (6) and (11))

$$\frac{k_3}{k_1} = \frac{Q_{\mathrm{KAP,M}}\, k_{\mathrm{M}}}{K_{\mathrm{c,air,centre}}\, A_{\mathrm{nom}}} = \frac{P_{\mathrm{KA,o}}}{K_{\mathrm{c.air,centre}}\, A_{\mathrm{nom}}} \approx \frac{P_{\mathrm{KA,o}}}{P_{\mathrm{KA,Anom}}}, \qquad (19)$$

where $K_{\mathrm{c,air,centre}}$ and A_{nom} are both measured at the patient entrance plane. In Paper IV the quotient in equation (19) was calculated using Monte Carlo simulations. The scattered radiation produced in the KAP-meter was traced and included in $P_{\mathrm{KA,o}}$ and $P_{\mathrm{KA,Anom}}$ as appropriate. In this geometry $P_{\mathrm{KA,Anom}}$ is closely related to the product $K_{\mathrm{c,air,centre}}\, A_{\mathrm{nom}}$. For a geometry similar to that in Figure 17 and a beam aperture of 9° (corresponding to a circular area with diameter 32 cm at 100 cm from the source), the quotient k_3/k_1 varied between 1.15 and 1.12 for tube voltages from 40 kV to 140 kV and was insensitive to the primary filtration of the beam, see Figure 26 (cases A and C). The quotient was about 3% higher for a small area beam (diameter 10 cm) than for a large area one (32 cm diameter) indicating that the fraction of photons outside the nominal beam area (A_{nom}) at the patient plane is larger for the small field. With an additional filter on top of the KAP-meter, the quotient varied between 1.24 and 1.20 for the same tube voltages. The energy dependences of k_3 and k_1 will thus be somewhat different.

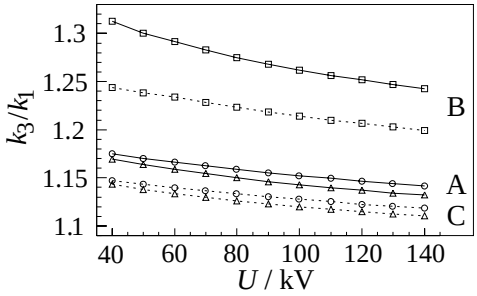

Figure 26. The quotient of the calibration coefficients k_3 and k_1 using calibration methods 3 and 1 (see text for explanation) as a function of the tube voltage, U. k_3/k_1 is calculated using data from Monte Carlo simulations (Paper IV) for different beam filtrations. Case A (○): Total filtration 5 mm Al, case B (□): An additional filter (2mm Al+0.15mm Cu) is placed in front of the KAP-meter. Case C (△): The additional filter was treated analytically as an ideal non-scattering filter (giving a total filtration of 7 mm Al+0.15 mm Cu). For each case, the quotient was calculated for two apertures 3° (___), and 9° (---) corresponding to circular beam areas with diameters 10 and 32 cm respectively 100 cm from the focal spot. The inverses of these data are also displayed in Figure 22 (a). (Figure from Paper V).

The relatively small energy dependence of the quotient k_3/k_1 shows that major variations of k_3 on tube voltage can be represented as variations of the reciprocal of the sensitivity (S^{-1}).

Calibration coefficients calculated by Monte Carlo simulations for exit and patient planes and for cases A, B, and C as a function of tube voltage (see section 6.2.2.) are shown in Table 3 and Figure 27.

Table 3. Absolute and relative values of the calibration coefficient, k, calculated by Monte Carlo simulations for beam aperture 6° and cases A, B, and C (see section 6.2.2.). Values of k_{60} correspond to a tube voltage of 60 kV. (From Paper IV). Case A: The additional filter was not used. Case B: The additional filter was placed closely in front of the KAP-meter. Case C: The additional filter was treated analytically as an ideal non-scattering filter. Primary filtration 5 mm Al; added filter 2 mm Al+0.15 mm Cu.

	U	Exit plane, $k=P_{KA,o}/Q_{KAP}$		Patient plane, $k=P_{KA,Anom}/Q_{KAP}$	
	U (kV)	k (Gym^2/C)	k/k_{60}	k (Gym^2/C)	k/k_{60}
A	40	1314	1.176	1118	1.168
A	90	1133	1.014	980	1.024
A	140	1272	1.139	1113	1.162
B	40	1139	1.141	873	1.123
B	90	1133	1.135	897	1.154
B	140	1347	1.349	1087	1.4
C	40	1140	1.126	974	1.117
C	90	1133	1.12	987	1.131
C	140	1378	1.362	1215	1.392

The differences between calibration coefficients obtained using different filtration, different positioning of the filter, and different reference planes shown in Figure 27 are discussed, below, see Paper IV for more details. The geometry shown in Figure 14 is helpful to use in analyzing the curves in Figure 27 and their dependence on the choice of reference plane. In general, when the patient plane and A_{nom} are used for deriving the calibration coefficient, ($k=P_{KA,Anom}/Q_{KAP}$) lower values are obtained than when the exit plane is used ($k=P_{KA,o}/Q_{KAP}$). This is due to obliquely scattered photons which pass through the KAP-meter exit plane, but impinge on the patient plane outside A_{nom}, thereby contributing to $P_{KA,o}$ but not to $P_{KA,Anom.}$ In the idealized Monte Carlo geometry, the only photons outside the primary beam (=A_{nom} in the patient plane) are those scattered in the filter, the KAP-meter, and air. The fraction of the scatter outside A_{nom} depends on many factors, e.g. the thickness of the filter and KAP-meter, the x-ray spectrum, the beam aperture and the distance between the "sources of scatter" and the patient plane. Cases A and C represent situations with different x-ray spectra (but all other factors equal) while cases B and C represent situations with (B) and without (C) an extra scattering filter close to the front of the KAP-meter (other factors again being equal).

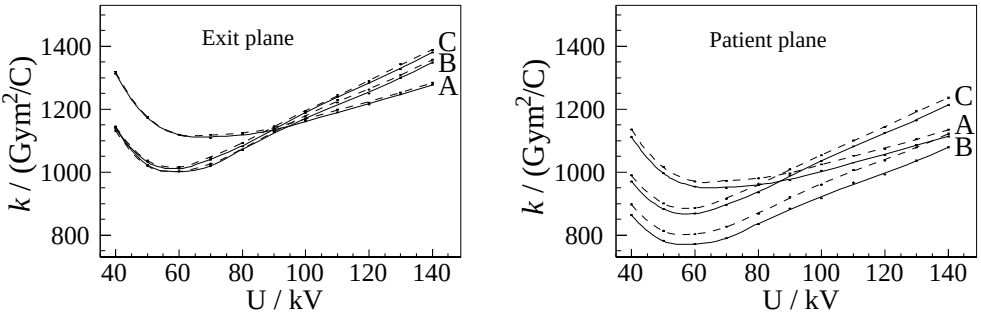

Figure 27. Calibration coefficients, $k = P_{KA}/Q_{KAP}$, as a function of tube voltage, U, for beam apertures 3° (——) and 12° (- - - -) in the exit and patient planes. Labels corresponding to cases A, B, and C are on the right side of each curve. Values for beam apertures of 6° and 9° lay in bands delimited by corresponding 3° and 12° aperture curves. Case A: No additional filter. Case B: Additional filter closely in front of KAP-meter. Case C: Additional filter treated analytically (Figure from Paper IV).

In both cases A and C, the decreases in k for the patient plane compared to the exit plane were similar and about 13-17% (the lower figure is for the higher tube voltage). The corresponding decrease in case B was about 18-24% due to scattered photons from the additional filter.

A difference of about 10% in the value of k_1 between cases B and C in the patient plane was not observed for k_3 (see Figure 27). This indicates that, even although a substantial amount (about 10%) of scattered photons passed obliquely through the KAP-

meter, their effect on the proportionality between $P_{KA,o}$ and Q_{KAP} was negligible. This is an important result. It shows that KAP-meters also measure obliquely incident photons with reasonable accuracy and that, compared to primary photons, the increased attenuation of scattered photons in the middle and exit electrodes of the KAP-meter is negligible for the actual range of angles.

The calibration coefficient curves for cases A and C show different variations with tube voltage. The x-ray spectra in case C are harder filtered and therefore narrower than the corresponding spectra for case A. When weighted over the curve of energy imparted shown in Figure 19, the narrower spectra give larger variations in Q_{KAP} when the tube voltage is changed, and thus larger variations in k.

6.5. Effects of added filters on KAP-meter calibration coefficients

Adding an extra filter in front of the KAP-meter causes a change in the energy spectrum of the primary photons and an increase of Q_{KAP} due to scattered photons from the filter. The fraction of scattered photons that pass through the KAP-meter depends on the distance between KAP-meter and filter. The effect on the calibration coefficients of positioning the filter closely in front of the KAP-meter was demonstrated in the Monte Carlo simulations in section 6.4.4. Results from measurement of the sensitivity, S, with a filter in front of the KAP-meter are shown in Figure 28. The KAP-meter signal increases as the distance between the filter and the KAP-meter decreases due to an increasing fraction of the scattered photons that reach the KAP- meter surface. The signal from the reference chamber (see Figure 17) was only slightly affected (less than 1.5%) by the position of the filter since the large air gap significantly reduced the amount of scatter at this distance.

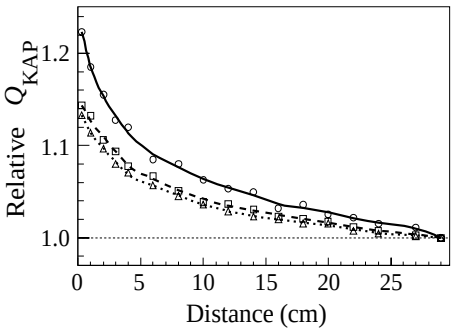

Figure 28. The relative signal of KM1 as a function of the distance from the test filter (2 mm Al+0.15 mm Cu) at three tube voltages; 40 (circle), 90 (box), and 140 kV (triangle). The total filtration (without the test filter) is 0.5 mm Al.

With a total filtration of 0.5 mm Al (without the test filter), the increase in the KAP-meter signal when the filter is introduced close to the KAP-meter, depends strongly on tube

voltage, the increase ranging from 14% at 140 kV to 22% at 40 kV. Using thicker primary filtration (3 mm Al), the increase was constant at 10% for tube voltages 40 - 140 kV, in accordance with the results from the Monte Carlo simulations in section 6.4.4 (using a total filtration of 5 mm Al but the same test filter, 2 mm Al + 0.15 mm Cu). Gfirtner *et al* (1997) used primary filtrations of "up to 2.5 mm Al" and an added filter (2 mm Al+0.1 mm Cu) inserted just above the KAP-meter. They examined the influence of the added filter on the calibration coefficient k_1 and found deviations of up to 25% (at tube voltage 70 kV). However, this cannot directly be compared to the 10% increase observed here (Figure 28) since Gfirtner *et al* measured the combined effect of both a change in the energy spectrum of the primary photons incident on the KAP-meter and of an increased amount of obliquely-scattered radiation detected by the KAP-meter. If the influence of the energy spectrum is taken into account (see Figure 24), a combined effect of up to 26% is obtained, in good agreement with the results from Gfirtner *et al*.

7. Estimation of uncertainties

The methods and concepts for evaluating and expressing the uncertainty were adopted from "Guide to the Expression of Uncertainty in Measurement" (ISO 1993). The grouping of the components in the uncertainty is made according to the way in which their values are estimated:

A. Those which are evaluated by applying statistical methods to a series of repeated determinations.
B. Those which are evaluated by other means.

The old classification system, classifying the uncertainties as random or systematic, does not always correspond simply to the new categories A and B and has therefore been avoided as much as possible here.

7.1. Uncertainty in the calibration coefficient, k_2

To facilitate analysis, k_2 in equation (2) was rewritten (substituting equation (10) into equation (2)) as:

$$k = \frac{V_{\text{ref}} \cdot c_2 \cdot C_{\text{ref}} \cdot RAK \cdot d \cdot s \cdot r}{V_{\text{KAP}} \cdot c_1} \qquad (20)$$

Here, *RAK* (relative area kerma) is the sum $\sum_i \left(\Delta A_i \frac{M_i}{M_{\text{centre}}} \right)$ and V_{ref}, c_2 and C_{ref} the electrometer reading and the calibration coefficients for the electrometer and reference chamber respectively. V_{KAP} is the electrometer reading of the KAP-meter and c_1 the electrometer calibration coefficient. Factor *d* corrects for possible differences in the distances from the source to the centre of the reference chamber and to the plane of the TLD measurements, *s* for the variation in sensitivity over the KAP-meter area (this being needed when using the calibration coefficient at other beam areas than that used in the calibration) and *r* for a possible deviation between interpolated values of *RAK* and true ones at tube voltages for which *RAK* was not measured. Factors *d*, *s* and *r* were given the value of unity. They were only introduced to permit evaluation of uncertainties arising from these causes.

Table 4. Estimated relative standard uncertainties (u_X/X) and relative variances $(u_X/X)^2$ for the factors involved in estimating the combined relative standard uncertainties in calibration coefficient k_2, $(u_c(k)/k)$, at a tube voltage of 80 kV. The last column gives the relative contribution of the individual relative variances to the total combined variance $(u_c(k)/k)^2$ (From Paper I)

X	$\left(\frac{u_X}{X}\right)$ (%)	$\left(\frac{u_X}{X}\right)^2$ (%)	Relative contribution to $\left(\frac{u_c(k)}{k}\right)^2$ (%)
RAK	1.29	0.02	70.0
V_{ref}	0.15	0.00	0.9
c_2	0.20	0.0004	1.7
d	0.22	0.0005	2.0
s	0.20	0.0004	1.7
r	0.50	0.0025	10.5
C_{ref}	0.36	0.0013	5.5
V_{KAP}	0.15	0.0002	0.9
c_1	0.4	0.0016	6.7
$\left(\frac{u_c(k)}{k}\right)^2$	=0.0238%		
$\left(\frac{u_c(k)}{k}\right)$	=1.5%		

Correlations between the quantities in Table 4 were assumed to be negligible and the combined relative variance in the calibration coefficient was obtained from ISO (1993):

$$\left(\frac{u_c(k)}{k}\right)^2 = \left(\frac{u(V_{ref})}{V_{ref}}\right)^2 + \left(\frac{u(c_2)}{c_2}\right)^2 + \left(\frac{u(C_{ref})}{C_{ref}}\right)^2 + \\ + \left(\frac{u(RAK)}{RAK}\right)^2 + \left(\frac{u(d)}{d}\right)^2 + \left(\frac{u(s)}{s}\right)^2 + \\ + \left(\frac{u(r)}{r}\right)^2 + \left(-\frac{u(V_{KAP})}{V_{KAP}}\right)^2 + \left(-\frac{u(c_1)}{c_1}\right)^2 \qquad (21)$$

A detailed description of the calculation of the relative variances of the factors in equation (7) is given in Paper II. The calculations are in many cases very easily performed. However, some calculations e.g. of *u(RAK)/RAK* are not straightforward, and extra assumptions must be made when carrying them out.

As seen from Table 4, the combined relative standard uncertainty, 1.5%, is dominated by the contribution from the relative standard uncertainty in *RAK* and better estimates of *RAK* would strongly reduce the uncertainty in k, $(u_c(k)/k)$.

7.2. Uncertainties in comparisons of calibration coefficients

The combined relative variances $(u_c(\Delta)/\Delta)^2$ were evaluated using the following expressions for $\Delta_{\text{sq.law}} = k_{1,\text{sq.law}}/k_2$ and $\Delta_{\text{film}} = k_{1,\text{film}}/k_2$:

$$\Delta_{\text{sq.law}} = \frac{V_{ref}\, c_2 C_{ref\Delta}\left[A_{col}\left(\frac{t_{ref}}{t_{col}} \right)^2 \right]}{kV_{\text{KAP}} \cdot c_1} \qquad (22)$$

$$\Delta_{\text{film}} = \frac{V_{ref}\, c_2 C_{\text{ref}\Delta} A_{\text{film}}}{kV_{\text{KAP}} c_1}$$

Here, V_{ref}, c_2, k, V_{KAP} and c_1 are as defined above; A_{col} is the opening area of the lead collimator and t_{col} and t_{ref} the distances from the source to the collimator and reference chamber respectively. $C_{\text{ref}\Delta}$ is the reference ionisation chamber calibration coefficient.

Table 5. Estimated maximum and minimum values of the relative combined variance $(u_c(\Delta)/\Delta)^2$ and the combined relative standard uncertainty $u_c(\Delta)/\Delta$ for calibration method 1.

	$(u_C(\Delta)/\Delta)^2$ (‰)		$(u_C(\Delta)/\Delta)$ (%)	
	Max	Min	Max	Min
Method 1, sq.law	0.833	0.420	2.9	2.1
Method 1, film	0.519	0.480	2.3	2.2

The combined relative variances in Δ_1 and Δ_2 are obtained from

$$\left(\frac{u_c\left(\Delta_{\text{sq.law}}\right)}{\Delta_{\text{sq.law}}}\right)^2 = \left(\frac{u(V_{\text{ref}})}{V_{\text{ref}}}\right)^2 + \left(\frac{u(c_2)}{c_2}\right)^2 + \left(\frac{u(C_{ref\Delta})}{C_{ref\Delta}}\right)^2 + \\ + \left(\frac{u(A_{col})}{A_{col}}\right)^2 + \left(2 \cdot \frac{u(t_{ref})}{t_{ref}}\right)^2 + \left(2 \cdot \frac{u(t_{col})}{t_{col}}\right)^2 + \\ + \left(-\frac{u(k)}{k}\right)^2 + \left(-\frac{u(V_{KAP})}{V_{KAP}}\right)^2 + \left(-\frac{u(c_1)}{c_1}\right)^2 \qquad (23)$$

$$\left(\frac{u_c\left(\Delta_{\text{film}}\right)}{\Delta_{\text{film}}}\right)^2 = \left(\frac{u(V_{\text{ref}})}{V_{\text{ref}}}\right)^2 + \left(\frac{u(c_2)}{c_2}\right)^2 + \left(\frac{u(C_{ref\Delta})}{C_{ref\Delta}}\right)^2 + \\ + \left(\frac{u(A_{film})}{A_{film}}\right)^2 + \left(-\frac{u(k)}{k}\right)^2 + \\ + \left(-\frac{u(V_{KAP})}{V_{KAP}}\right)^2 + \left(-\frac{u(c_1)}{c_1}\right)^2 \qquad (24)$$

Different values of the combined relative variance in $\Delta_{\text{sq.law}}$ and Δ_{film} are obtained at different tube voltages, distances and collimator apertures. Detailed evaluations of the components in equations (23) and (24) used in calculating the combined standard uncertainties are given in Paper II.

It should be pointed out that the estimation of A_{film} was carried out using a microdensitometer and at optical densities of the x-ray film not exceeding 0.5 ODU. This resulted in a much smaller uncertainty than would be expected from Figure 3 and Figure 4, which show the additional uncertainties introduced using other means of determining A_{film}.

7.3. Uncertainties in the workshop calibration coefficient

Since calibration coefficients (k_{w}) at the Linköping workshop were derived by comparison with a well-calibrated KAP-meter, the uncertainty in k_{w} is larger than that of k_2 described in section 7.1. k_{w} was determined as

$$k_{\text{w}} = \frac{\left(\frac{V}{V_{ref}}\right) kr}{\left(\frac{V_w}{V_{ref_w}}\right)} \qquad (25)$$

V , k and V_{ref} are the KAP-meter reading, the calibration coefficient and the reading of the chamber used for normalization, respectively and r = 1 is introduced to represent the uncertainty in the calibration coefficient k due to the uncertainty in the radiation quality. V_w and V_{refw} are the corresponding readings from the KAP-meter to be calibrated.
Varying relative combined standard uncertainties were obtained. The values ranged from 1.9% to 2.8% and depended on tube voltage and on the stability of the electrometer used to measure V_w. The relative combined standard uncertainties were obtained from

$$\left[\frac{u_c(k_w)}{k_w}\right]^2 = \left[\frac{u\left(\frac{V}{V_{ref}}\right)}{\left(\frac{V}{V_{ref}}\right)}\right]^2 + \left[\frac{u\left(\frac{V_w}{V_{ref_w}}\right)}{\left(\frac{V_w}{V_{ref_w}}\right)}\right]^2 + \left[\frac{u(k)}{k}\right]^2 + \left[\frac{u(r)}{r}\right]^2 \qquad (26)$$

assuming that correlations between the quantities in equation (25) were negligible.

7.4. Expanded uncertainty

The expanded uncertainty (U) is obtained by multiplying the combined standard uncertainty with a coverage factor, c_p, giving an interval with confidence p ($U=c_p u_c(k)$). Lack of knowledge of the input estimates prevents rigorous estimate of c_p for a specified level of confidence. The most elementary approach yielding $c_{95\%}$= 2 and $c_{99\%}$ = 3, was therefore adopted (ISO 1993).

7.5. Uncertainties in reported P_{KA}-values

For use in setting of diagnostic reference levels (DRL), results of P_{KA} measurements are reported to the national radiation protection authority. To make comparison of reported values meaningful, it is necessary to be able to keep track of the calibration coefficients that have been used in the different hospitals when converting measured KAP-meter signals to values of P_{KA}. The uncertainty in reported P_{KA} -values depends on several factors. The calibration method used by the hospital physicists to derive the calibration coefficients is one important factor. The large energy dependence of the calibration coefficients, if not corrected for, causes the uncertainty in reported values of P_{KA} to increase further. To facilitate an estimation of the uncertainty in reported values, the following information should be provided: (1) A description of the calibration method (2) Specification of the radiation quality at which the calibration coefficient used is valid (e.g. tube voltage and filtration or tube voltage and HVL). (3) Specification of the range of tube voltages and

filtrations used in the measurements. (4) Specification of eventual correction factors applied at undercouch installations. (5) Specification of positions of added filters. (6) Specification of the type of KAP-meter used. Below, two examples of possible uncertainties are given.
Practitioners A and B, with identical indium oxide coated KAP-meters, measure the P_{KA} at the same x-ray examination. The signals, Q_{KAP}, obtained by both practitioners are thus the same. Suppose that practitioner A has a KAP-meter with calibration coefficients k_2 (obtained using calibration method 2) so that measured P_{KA}-values are in terms of $P_{KA,o}$. Practitioner B uses calibration method 1 to derive values of k_1 yielding values in terms of $P_{KA,Anom}$. The following describes two extreme cases (case 1 and 2) in which practitioner A and B report P_{KA}-values that differ considerably from each other:

(1) The x-ray examination was made using a high tube voltage (140 kV) with a total filtration of 5 mm Al+0.15 mm Cu. Practitioner B measured $K_{c,air,centre}$ at a large distance (140 cm) from the focal spot using a relatively small beam area (about 115 cm^2 at 140 cm) to determine k_1. Due to this choice of geometry and calibration method, a value of k_1 17% lower than that of k_2 is obtained (Figure 10). If an additional filter (2 mm Al + 0.15 mm Cu) was positioned in front of the KAP-meter, the values of k_1 obtained by practitioner B decreases by an additional 10% as compared to values of k_2 (Figure 27 and Figure 28). If, in addition, practitioner B used a single value of the calibration coefficient k_1 determined at the tube voltage 70 kV an additional decrease relative to k_2 of 13% is obtained (Figure 24). Altogether this results in values of P_{KA} reported by practitioner B ($P_{KA} = K_{c,air,centre}A_{nom} \approx P_{KA,Anom}$) that are about 40% lower than those reported by practitioner A ($P_{KA} = P_{KA,o}$) who correctly accounted for the beam quality used.

(2) The x-ray examination was made using medium tube voltages (60-80 kV) and a total filtration of 5 mm Al+0.15 mm Cu. Practitioner B derived the calibration coefficient k_1 using a large field (300 cm^2) and a short distance (50 cm) from the focal spot, resulting in values of k_1 that are 8% higher than those of k_2 (Figure 9). If practitioner B used the value of k_1 at 140 kV, an additional increase in k_1 (as compared to k_2) of 13% is obtained and the P_{KA}-values reported by practitioner B are about 21% higher than those reported by practitioner A. If, in addition, the examination was made at an undercouch installation and if practitioner A did, but practitioner B did not, correct for the influence on the calibration coefficients from attenuation and scatter in the couch and cushion, the deviation between the reported values of P_{KA} from practitioner A and B will increase further.

8. Radiation risk and P_{KA}

8.1. $P_{KA,patient}$

The quantity $P_{KA,patient}$ is here introduced as the air collision kerma at the patient entrance plane integrated over the area traversed by photons hitting the patient and has, in general, the best possible correlation to radiation risk. $P_{KA,patient}$ depends on the individual patient and x-ray installation and is difficult to estimate in clinical practice. In $P_{KA,Anom}$ the area of integration is restricted to within the area of the primary beam. Extra-focal radiation and photons scattered in the KAP-meter and added filters may hit the patient although passing outside A_{nom} so that $P_{KA,Anom}$ underestimates $P_{KA,patient}$. $P_{KA,o}$, on the other hand, includes all the extra-focal radiation and photons scattered in KAP-meter and filters, part of which are likely to pass outside the patient. A schematic view of the mutual relation between $P_{KA,Anom}$, $P_{KA,patient}$ and $P_{KA,o}$ is shown in Figure 29. The distance between $P_{KA,Anom}$ and $P_{KA,o}$ (i.e. the difference between their values) depends on several factors, the amount of scattered and extra-focal radiation and their distribution in the patient plane, collimator construction, beam area, distance from the patient plane to filter and KAP-meter, and tube voltage. Values of $P_{KA,o}$, as estimated from the values of calibration coefficients in Table 3, are between 14 and 17% higher than those of $P_{KA,Anom}$. When adding an extra filter close to the KAP-meter the values of $P_{KA,o}$ are about 24-30% higher than the corresponding values of $P_{KA,Anom}$. The given percentages were calculated as $(P_{KA,Anom}-P_{KA,o})/P_{KA,Anom}$.

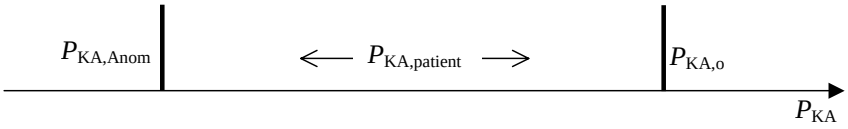

Figure 29. Schematic view of the relation between $P_{KA,patient}$, $P_{KA,Anom}$ and $P_{KA,o}$. The position of $P_{KA,patient}$ in between $P_{KA,Anom}$ and $P_{KA,o}$ depends on several factors, e.g. patient size, size of beam area, position of the beam on the patient. $P_{KA,Anom}$ always underestimates the value of $P_{KA,patient}$ while $P_{KA,o}$ overestimates it.

The actual position of $P_{KA,patient}$ in between $P_{KA,Anom}$ and $P_{KA,o}$ depends on factors that influence on the fraction of photons that pass outside A_{nom} but still hit the patient such as patient size, position of the beam on the patient, size of A_{nom} , distance between patient plane and the filter and KAP-meter.

Generally, $P_{KA,Anom}$ is believed to be closer to $P_{KA,patient}$ compared to $P_{KA,o}$. However, if it is important not to underestimate $P_{KA,patient}$, $P_{KA,o}$ is the best choice and has other advantages as well. As mentioned in section 2.3., P_{KA} is one of the quantities for reporting Diagnostic Reference Levels (DRL). A harmonization of the definition of P_{KA} and of calibration procedures would facilitate the comparisons of P_{KA} –values reported from

different practitioners, hospitals, and regions. A system with calibration of clinical KAP-meters using a Master KAP calibrated at a standard laboratory (method 3) has many advantages. One Master KAP-meter can be used at each hospital to calibrate the clinical KAP-meters according to a standardized calibration protocol to ensure congruence in measured P_{KA} –values between different hospitals. I this case $P_{KA,o}$ is suitable to use since, contrary to $P_{KA,Anom}$, it does not depend on the actual irradiation geometry. When a more precise estimation of radiation risk is needed, e.g., for a special patient or type of x-ray examination, it may be possible to estimate $P_{KA,patient}$ from $P_{KA,o}$ taking into account the amount of radiation from both the primary beam and extra-focal and scattered radiation passing outside the patient.

8.2. Conversion to risk related quantities

Even if $P_{KA,patient}$ can be accurately determined, this quantity alone cannot be used in optimization procedures but has to be converted to a risk related quantity. Wise *et al* (1999) showed that P_{KA} provides a good measure of the energy imparted, ε, to the patient, being robust to variations in patient size and sex as well as to variations in field size and beam quality within reasonable limits occurring in practice. Conversion coefficients ε/P_{KA} have been published and discussed by many authors (Carlsson 1963, Carlsson 1965b, Alm Carlsson *et al* 1984, Persliden and Sandborg 1993, Alm Carlsson *et al* 1999). It may also be interesting to investigate a direct conversion of Q_{KAP} to ε. Such a conversion factor, denoted $C_{Q,\varepsilon,}$ can be derived from

$$C_{Q,\varepsilon} = \frac{\varepsilon}{Q_{KAP}} = \frac{\varepsilon}{P_{KA}} k\,, \tag{27}$$

where k is the KAP-meter calibration coefficient with respect to P_{KA} . The value of the energy imparted to the patient is then obtained as

$$\varepsilon = \frac{\varepsilon}{P_{KA}} P_{KA} = C_{Q,\varepsilon} Q_{KAP}\,. \tag{28}$$

In Figure 30 an example of the conversion coefficients $C_{Q,\varepsilon}$ are shown as a function of HVL in aluminium for examinations of the adult trunk. The ε/P_{KA} –values were published in Carlsson and Alm Carlsson (1990) as calculated from data from Jones and Wall (1985). The KAP-meter calibration coefficients, k_2, were taken from Figure 7 (Paper I).

The conversion coefficient $C_{Q,\varepsilon}$ increases with increasing HVL, however, with an energy dependence for the KM1 that is clearly smaller compared to that of the graphite

coated KM2 and to the conversion coefficients ε/P_{KA}. It is interesting to note that although the energy dependence of the P_{KA} calibration coefficient for KM2 is considerably smaller than that for KM1, the opposite is true for the conversion coefficient $C_{Q,\varepsilon}$.

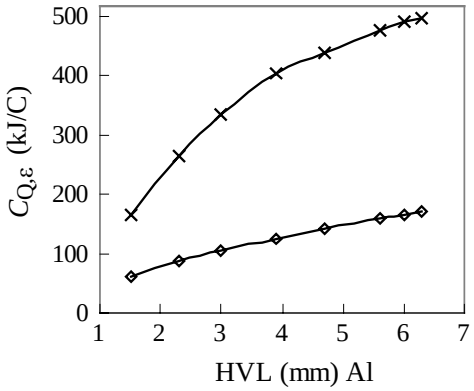

Figure 30. Values of the conversion coefficient $C_{Q,\varepsilon}$ as a function of HVL in aluminium for KM1 (◇) and KM2 (×). Values of $C_{Q,\varepsilon}$ were calculated from published conversion coefficients ε/P_{KA} for examinations of the adult trunk (Carlsson and Alm Carlsson 1990) and the KAP-meter calibration coefficients, k_2, (Figure 7) derived in Paper I for KM1 and KM2.

The energy dependence of KAP-meter measurements generally focus on the energy dependence of the calibration coefficients (k). An interesting alternative is to focus instead on the energy dependence of $C_{Q,\varepsilon}$. This was first proposed by Carlsson (1965a) who made attempts to construct a KAP-meter that was energy independent with respect to measurements of integral dose (energy imparted to the patient). He stated that the energy dependence could be varied within wide limits by varying the thickness of the coating and air layer and by varying the atomic number of the coating. However, he found the task to complex and abandoned it. Today, with the use of Monte Carlo simulations, it is possible to quickly test the influence from any coating and the task to construct a KAP-meter with values of $C_{Q,\varepsilon}$ that are fairly constant may succeed. For example, it may be advantageous to use a material with higher atomic number than indium (Z=49), e.g. gold (Z=79). The peak shown in Figure 19 (for In_2O_3) is then expected to be shifted towards higher photon energies. This is also the case for the valley of the calibration curve (see Figure 7, KM1). If the resulting calibration coefficient (k) for such a KAP-meter decreases constantly with increasing tube voltage (within the range of clinical tube voltages), the product k times ε/P_{KA} may be fairly constant since ε/P_{KA} increases with increasing tube voltage. The light transparency of the KAP-meter may be affected by using conducting layers of a high atomic number material. However, a layer of gold less than 5 nm is transparent to light, is conducting, and possible to manufacture ((Hultman 2006). Light transparency is also not a concern at undercouch installations or in fluoroscopy.

9. Summary

The factors influencing the accuracy of the calibration coefficients $k = P_{KA}/Q_{KAP}$ and of reported P_{KA}-values were analyzed in detail. In addition, the energy dependence of the calibration coefficients was investigated using both Monte Carlo simulations and measurements.

Due to attenuation and scatter in the KAP-meter and presence of extra-focal radiation, values of P_{KA} depend on the choice of integration area A and the distance of the reference plane from the focal spot yielding values of P_{KA} that may differ by as much as 23% depending on this choice. The two extremes correspond to (1) $P_{KA}=P_{KA,o}$ integrated over the exit surface of the KAP-meter resulting in geometry independent calibration coefficients and (2) $P_{KA}=P_{KA,Anom}$ integrated over the nominal beam area A_{nom} in the patient entrance plane resulting in geometry dependent calibration coefficients.

Three calibration methods were analysed. Method 1 aims at determination of $P_{KA,Anom}$ approximated by the product of $K_{c,air,centre}$ and A_{nom} measuerd in the patient entrance plane. Values of the corresponding calibration coefficients were found to depend on the size of A_{nom} and the distance of the patient plane from the focal spot. It could be shown that this was caused by a varying degree of escape of extra-focal radiation out of A_{nom}. At standard laboratories, the method is used to perform calibrations with respect to the radiation incident on the KAP-meter. Problems with beam inhomogeneity, extra-focal and scattered radiation are avoided resulting in calibration coefficients with low standard uncertainty (±1.5 %, coverage factor 2). A KAP-meter calibrated this way is called a Master KAP-meter. Method 2 was designed in this work to approach determination of $P_{KA,o}$ using thermoluminescent detectors to monitor contributions from extra-focal radiation and account for the heel effect. The uncertainty in derived calibration coefficients was ± 3% (coverage factor 2). Method 3 uses a Master KAP-meter to calibrate clinical KAP-meters. It has potential to become the standard method in the future replacing the tedious method 2 for calibrations aiming at determination of $P_{KA,o}$.

Calibration coefficients for commercially available KAP-meters with conducting layers of indium oxide exhibit a strong energy dependence. This dependence was investigated using both Monte Carlo simulations and measurements. It may introduce substantial uncertainties in reported P_{KA}– values since calibration coefficients as obtained from standard laboratories are often available only at one filtration (2.5 mm Al) as function of tube voltage or HVL. This is not sufficient since higher filtrations are commonly used in practice, including filters of Cu. In extreme cases, calibration coefficients for the same value of HVL but using different tube voltages and filtrations can deviate by as much as 30%. The energy dependence is considerably reduced using graphite coated KAP-meters.

Calibration coefficients $C_{Q,\varepsilon} = \varepsilon/Q_{KAP}$ where ε is the energy imparted to the patient were also derived. Contrary to the P_{KA} calibration coefficients k, the calibration coefficients $C_{Q,\varepsilon} = \varepsilon/Q_{KAP}$ show a considerably larger energy dependence for the graphite coated chambers compared to those for indium oxide coated chambers. To achieve a flat energy response of $C_{Q,\varepsilon} = \varepsilon/Q_{KAP}$, still higher atomic number coatings would possibly be needed.

10. Conclusions

The energy dependence in the calibration coefficients for commercially available KAP-meters is considerable and caused by the high atomic number coating (indium oxide) of the KAP-meter walls. Calibration coefficients as obtained from standard laboratories are often given as a function of tube voltage or HVL for beams with 2.5 mm aluminium. This is not sufficient for clinical applications where thicker filtrations are frequently used, including filters of Cu. In extreme cases, calibration coefficients may differ by as much as 30% for the same value of HVL but using other tube voltages and filtrations.

Due to extra-focal radiation and scatter from the KAP-meter, values of P_{KA} depend on the choice of integration area and reference plane. Calibration coefficients derived with respect to $P_{KA,Anom}$ deviate from those derived with respect to $P_{KA,o}$ by 12-30% in the investigated calibration geometries. $P_{KA,Anom}$ is the air kerma integrated over the nominal beam area A_{nom} in the patient entrance plane; $P_{KA,o}$ is the air kerma integrated over the exit plane of the KAP-meter and is closely related to the KAP-meter signal Q_{KAP} even in cases when an additional filter is positioned close to the KAP-meter. Calibration coefficients relative to $P_{KA,o}$ are independent of the irradiation geometry whereas calibration coefficients relative to $P_{KA,Anom}$ depend on the calibration geometry and the actual x-ray installation. Therefore, when using KAP-meters for fluoroscopy where the focus-skin distance varies during the examination, calibration coefficients relative to $P_{KA,o}$ should be preferred. If used to estimate patient risk from KAP-meter measurements, $P_{KA,Anom}$ underestimates and $P_{KA,o}$ overestimates $P_{KA,patient}$, the air kerma at the patient entrance plane integrated over the area where incident photons subsequently hit the patient.

To increase the uniformity in values of calibration coefficients used in clinical measurements and of reported P_{KA}-values, it would be advantageous to calibrate clinical KAP-meters using a Master KAP-meter and a well-specified calibration protocol, aiming at a determination of $P_{KA,o}$. This would also facilitate the work by hospital physicists who have to perform measurements of P_{KA} at a large number of x-ray installations in different hospitals.

The results presented in this work show that if standardised calibration methods are not used and choice of calibration coefficients not carefully selected with respect to beam quality, the total uncertainty in reported P_{KA}-values may be as large as 40-45%. This should be compared to the goal of an accuracy of 7 % (coverage factor 2) for dose measurements in diagnostic radiology set up by IAEA (2006). For KAP-meter measurements during fluoroscopy, where the tube voltage may vary during the examination, efforts should be taken to reduce the uncertainty to less than 25%.

11. Future work

The following issues are of interest for further investigations:

The influence of the extra-focal radiation on the calibration coefficients obtained using different calibration methods and the influence from the extra-focal radiation on the conversion of reported P_{KA} values to risk related quantities requiring mapping of the amount of extra-focal radiation and its distribution in different reference planes.

The energy dependence of calibration coefficients P_{KA}/Q_{KAP} and ε/P_{KA} . While a flat response of P_{KA}/Q_{KAP} seems to require coatings with effective atomic number close to that of air, a flat response of ε/P_{KA} may need a high atomic number coating material to compensate for the energy dependence of ε/P_{KA}.

The influence of the size of the beam area and the distance between the Master KAP and the clinical KAP- meter on the calibration coefficient using calibration method 3 aiming at achieving a geometry independent calibration coefficient approximating $k = P_{KA.o}/Q_{KAP}$. This means minimizing the escape of photons exiting from the clinical KAP-meter, which will not be registered by the Master KAP and the influence on the KAP-meter signals due to photons scattered between the KAP-meters. Factors to correct for these effects may also be established.

Calibration coefficients valid for undercouch installations. Such calibration coefficients are usually derived applying a factor to account for the attenuation in the patient couch. However, scattered radiation from the couch will also reach the patient and the distribution of scattered photons in the patient entrance plane and its effect on P_{KA} needs investigation.

In all cases, Monte Carlo simulations offer a useful tool for the suggested investigations. Regards the studies of the effects of extra-focal radiation, a model of the source of extra focal photons needs to be developed.

It is noted that in the recently published “Code of Practise for Dosimetry in Diagnostic Radiology by the IAEA (2006), the goal for the accuracy (coverage factor 2) in dose measurements are

- 7% for in-beam measurements;
- 20% for radiation survey measurements.

For some investigations, e.g., research, narrower limits of uncertainty may be required.
To fulfil these requirements on the accuracy of dose measurements, the investigations suggested here will be highly needed.

Acknowledgements

I wish to express my deep and sincere gratitude to:

- Professor Gudrun Alm Carlsson, my main supervisor, for her continuous support in all aspects of the work presented in this thesis. Her patience with ignorant PhD-students and remarkable ability to quickly penetrate any subject are very much appreciated. None of the manuscripts would have come even close to what they are without her active collaboration.

-Alexandr Malušek for his invaluable contributions to solving the problems with reference planes and areas of integration, for pointing out the connection between $\int_{\infty} K_{c,air} dA$ and outer space (I have always been interested in astrophysics) and for interesting discussions of life, love and the sexual behaviour of elephants.

- Professor Jan Persliden, my supervisor, for his encouragement and especially for keeping telling me "Just do it and do it now!".

- Professor emeritus Carl Carlsson for encouraging and constructive discussions during the initial work of this thesis. In many of his papers about KAP-meters, written more than 40 years ago, “grains of gold” are still found.

- Dr. Michael Sandborg for always being there to support with his great knowledge, expertise, and friendship.

- Dr. Ebba Helmrot for her inspiring words when I thought my supervisors and me were the only ones in the world interested in KAP-meter calibrations.

- All colleagues at the Department of Radiation Physics for making it such a stimulating and pleasant place to work at. Special thanks are due to Sara Olsson who took charge of the Radiation Therapy Section during my final work with his thesis, to Jalil Bahar-Gogani and Anna Olsson for their concern, to Håkan Gustafsson for guidance on Adobe Illustrator, and to Gustaf Ullman who bought all the tea I consumed during the final preparation of this thesis.

- All my colleagues at the Department of Radiation Therapy, especially to Mr. Bernt Karlsson and Mr. Hans Johansson for help and advice in all kinds of mechanical and electrical matters.

- Dr. Peter Dougan for the linguistic revision of this thesis.

- My ex-wife Petra who did a lot more housekeeping than I during some early intensive periods of this work and to her father, Bo, who made me understand the value of being well-educated.

- My father as the one who introduced me into the world of science. His fascination and enthusiasm for physics were the main reason for my early interest in this subject.

Finally, I would like to thank Madelene for all her love, patience and support during the preparation of this thesis. You are outstanding in so many respects!

References

Alm Carlsson G 1985, *Theoretical Basis for Dosimetry,(The Dosimetry of Ionizing Radiation)* Vol. I K R Kase, B E Bjärngard and F H Attix, (Orlando: Academic Press) pp. 1-75

Alm Carlsson G, Carlsson C A and Persliden J 1984 Energy imparted to the patient in diagnostic radiology: calculation of conversion factors for determining the energy imparted from measurements of the air collision kerma integrated over beam area *Phys. Med. Biol.* **29** 1329-1341.

Alm Carlsson G, Dance D R, Persliden J and Sandborg M 1999 Use of the concept of energy imparted in diagnostic radiology *Applied Radiation and Isotopes* **50** 39-62.

Ardran G M and Crooks H E 1978 Penetrameter cassette calibration to 400 kV and effects of extra-focal radiation when measuring tube filtration *Br. J. Radiol.* **51** 29-34.

Baró J, Sempau J, Fernandez-Varea J M and Salvat F 1995 PENELOPE: An algorithm for Monte Carlo simulation of the penetration and energy loss of electrons and positrons in matter *Nuclear Instruments and Methods in Physics Research Section B: Beam Interactions with Materials and Atoms* **100** 31-46.

Bednarek D R and Rudin S 2000 Comparison of two dose-area-product ionization chambers with different conductive surface coating for over-table and under-table tube configurations. *Health. Phys.* **78** 316-321.

Carlsson C 1963 Determination of integral absorbed dose from exposure measurements *Acta. Radiol. Ther. Phys. Biol.* **1** 433-458.

Carlsson C 1965a Integral Absorbed Doses in Roentgen Diagnostic Procedures. I. The Dosemeter *Acta. Radiol. Ther. Phys. Biol.* **177** 310-326.

Carlsson C 1965b Integral absorbed doses in roentgen diagnostic procedures. II. Measurement of integral doses in two roentgen diagnostic departments *Acta. Radiol. Ther. Phys. Biol.* **3** 384-408.

Carlsson C 1996, 'Personal communication'.

Carlsson C A and Alm Carlsson G 1990, *Dosimetry in Diagnostic Radiology and Computerized Tomography,(The Dosimetry of Ionizing Radiation)* Vol. 3 K R Kase, B E Bjärngard and F H Attix, (Orlando: Academic Press) pp. 163-257

Cranley K, Gilmore B J, Fogarty G W A and Desponds L 1997, *Catalogue of Diagnostic X-ray Spectra and Other Data, CD-Rom Edition Report* 78 (York:The Institute of Physics and Engineering in Medicine, IPEM)

Edholm P 1982 Exaggerated fear of radiation is a widely spread phobia (in Swedish) *Läkartidningen* **79** 4382-4383.

EUR 1996a, *European Guidelines on Quality Criteria for Diagnostic Radiographic Images, Report* EUR 16260 EN (Luxemburg:Office for Official Publications of the European Communities)

EUR 1996b, *European Guidelines on Quality Criteria for Diagnostic Radiographic Images in Paediatrics, Report* EUR16261 EN (Luxemburg:Office for Official Publications of the European Communities)

EuropeanCouncil 1997, *Council Directive 97/43/Euratom of 30 June 1997 on health protection of individuals against the dangers of ionising radiation in relation to medical exposure, and repealing Directive 84/866/Euratom,* Official Journal of the European Community L180, 40:0022–7

FDA 1994, *Avoidance of Serious X-ray-Induced Skin Injuries to Patients During*

Fluoroscopically-Guided Procedures, Food and Drug Administration (Rockville, MD:Center for Devices and Radiological Health)

Gfirtner H, Stieve F E and Wild J 1997 A new Diamentor for measuring kerma-area product and air-kerma simultaneously *Med. Phys.* **24** 1954-1959.

Grindborg J-E 2006, 'Personal communication'.

Hansson J 2006, 'Personal communication'.

Hart D, Jones D G and Wall B F 1994, *Estimation of Effective Dose in Diagnostic Radiology from Entrance Surface Dose and Dose-Area Product Measurements, Report* NRPB-R262 (Chilton:The National Radiological Protection Board, NRPB)

Hart D, Jones D G and Wall B F 1996, *Coefficients for Estimating Effective Doses from Paediatric X-ray Examinations, Report* NRPB-R279 (Chilton:The National Radiological Protection Board, NRPB)

Hart D and Wall B F 1994 Estimation of effective dose from dose-area product measurements for barium meals and barium enemas *Br. J. Radiol.* **67** 485-489.

Hultman L 2006, 'Personal communication'.

IAEA 2006, *Dosimetry in Diagnositic Radiology. An International Code of Practise, In print*

ICRP 1991, *Recommendations of the International Commission on Radiological Protection, Ann. ICRP 21* ICRP Publication 60 (Oxford:Pergamon)

ICRP 1996, *Radiological protection and safety in medicine, Ann. ICRP 26* ICRP Publication 73

IEC 1977, *Area Exposure Product Meter, International Electrotechnical Commission, IEC Standard* International Electrotechnical Commission, IEC 580, First edition

ISO 1993, *Guide to the Expression of Uncertainty in Measurement,* International Organization for Standardization

Jones D and Wall B F 1985, *Organ Doses from Medical X-ray Examinations Calculated using Monte Carlo Techniques, Report* NRPB-R186 (London:The National Radiological Protection Board, NRPB)

Koenig T R, Mettler F A and Wagner L K 2001 Skin injuries from fluoroscopically guided procedures: part 2, review of 73 cases and recommendations for minimizing dose delivered to patient *Am. J. Roentgenol.* **177** 13-20.

Larsson J P, Persliden J, Sandborg M and Carlsson G A 1996 Transmission ionization chambers for measurements of air collision kerma integrated over beam area. Factors limiting the accuracy of calibration *Phys. Med. Biol.* **41** 2381-2398.

Le Heron J C 1992 Estimation of effective dose to the patient during medical x-ray examinations from measurements of the dose-area product *Phys. Med. Biol.* **37** 2117-2126.

Leitz W 2004 Personal communication.

Leitz W and Jönsson H 2001, *Patient doses from X-ray examinations in Sweden (In Swedish),* (Stockholm:Swedish Radiation Protection Institute)

Månsson L G, Wallström E and Mattsson S 1993 Relations between effective dose, effective dose equivalent, area-kerma product, and energy imparted in chest radiography *Radiation Protection Dosimetry* **49** 421-431.

NRPB 1990, *Patient dose reduction in diagnostic radiology,* (Chilton:The National Radiological Protection Board)

NRPB 1992, *National Protocol for Patient Dose Measurements in Diagnostic Radiology,* (Chilton:The National Radiological Protection Board)

Persliden J and Sandborg M 1993 Conversion factors between the energy imparted to the patient and air collision kerma integrated over beam area in paediatric radiology *Acta. Radiol.* **34** 92-97.

Pychlau H and Pychlau P 1964 Ein Diagnostik-Dosimeter- Grundform und Abwandlung *Deutsche Röntgenkongr. Beiheft. Fortschr. Röntgenstr.* **100** 177-180.

Shrimpton P C and Wall B F 1982 An evaluation of the Diamentor transmission ionisation chamber in indicating exposure-area product (R cm2) during diagnostic radiological examinations *Phys. Med. Biol.* **27** 871-878.

Tapiovaara M, Lakkisto M and Servomaa A 1997, 'PCXMC - A PC-based Monte Carlo program for calculating patient doses in medical x-ray examinations, ' Finnish Centre for Radiation and Nuclear Safety (STUK). STUK-A139, Helsinki.

Wise K N, Sandborg M, Persliden J and Carlsson G A 1999 Sensitivity of coefficients for converting entrance surface dose and kerma-area product to effective dose and energy imparted to the patient *Phys. Med. Biol.* **44** 1937-1954.